Master's Thesis

SENSITIVITY ANALSIS OF PROCESS PARAMETERS CONSIDERING DIMENSIONAL ACCURACY AND RELATIVE DENSITY IN DIRECT ENERGY DEPOSITION WITH SUS316L POWDERS

Ga-Hyung Kim

Department of Mechanical Engineering

Graduate School of UNIST

2020

SENSITIVITY ANALSIS OF PROCESS PARAMETERS CONSIDERING DIMENSIONAL ACCURACY AND RELATIVE DENSITY IN DIRECT ENERGY DEPOSITION WITH SUS316L POWDERS

Ga-Hyung Kim

Department of Mechanical Engineering

Graduate School of UNIST

Sensitivity Analysis of Process Parameters considering Dimensional Accuracy and Relative Density in Direct Energy Deposition with SUS316L Powders

A thesis

submitted to the Graduate School of UNIST

in partial fulfillment of the

requirements for the degree of

Master of Science

Ga-Hyung Kim

12.24.2019

Approved by

Advisor

Namhun Kim

Sensitivity Analysis of Process Parameters considering Dimensional Accuracy and Relative Density in Direct Energy Deposition with SUS316L Powders

Ga-Hyung Kim

This certifies that the thesis of Ga-Hyung Kim is approved.

12/24/2019

Advisor: Namhun Kim

Duck Young Kim

Young-Bin Park

Abstract

This study aims to analyze fundamental parameters of the Direct Energy Deposition (DED) process on a single-track level, whereas previous studies typically used bulk models to directly investigate the effects of process parameters on final products. Grounded on the fact that a printed product is the horizontal and vertical aggregations of single tracks, the effect on width, height and relative density of the printed part is collected by input process parameters (laser power, powder feed rate and coaxial gas rate) on a divided scale across single track, multi-track and multi-layer. All specimens are printed on the fixed experimental setting of the DED machine (i.e., MX-600) of which powder and substrate are SUS316L. The significance of the input process parameters is statistically analyzed on the key output of each scale. Then, the optimal parameters for the final product are compared to the parameters derived from the bulk samples. The optimal parameters derived from bulk samples and multi-scale samples have the almost same values in terms of their influences on the variance of the target property, while the cost for printing the multi-scale samples decreases by about 83%. DED has recently emerged as a key tool in product manufacturing beyond mold repair in the metal 3D printing sector. However, due to the nature of the DED process, it is difficult to apply it as an industry in terms of cost by using high-volume metal powder and high-power laser source. In this sense, this research is expected to benefit for industrial applications of the DED process through its optimization using single-track sampling.

Contents

List of Figures

List of Tables

1. Introduction

1.1 Background

Recently, much attention has been focused to the Fourth industrial revolution, which began in German policy Industry 4.0. Industry 4.0 is a policy that combines manufacturing with ICT systems to move away from traditional centralized control to a distributed control system smart factory that networks production facilities. Additive Manufacturing (AM), defined as "the process of joining materials to make parts from 3D model data, usually layer upon layer, as opposed to subtractive and formative manufacturing methodologies" by ISO/ASTM 52900 [1], is considered an essential technology of the Fourth industrial revolution with the strength of multi-category small-volume production.

The various material available for AM systems is impressive. A designer can choose from a wide range of materials in plastics, ceramics, composites, metals, biomaterials, and glass. Among other things, metal AM shows remarkable growth in the aerospace and automotive industries. Powder Bed Fusion (PBF) and Direct Energy Deposition (DED) processes are typically capable of producing parts in the metals listed previously. Most DED systems can process an even wider range of materials. Some also have a multi-material capability, where combinations of two or more metals are possible. [1].

The biggest problem with metal AM components is that failure to completer density recues fracture toughness and fatigue strength. Porosity also plays a role in the beginning of crack, which can lead to failure of the part. Mechanical properties of DED parts depends on the process parameters which affect the microstructure and geometric shape. Optimization of the process parameter is important to avoid defects. The optimization process requires extensive experiments, which need high experimental cost and substantial time investing. It is difficult to develop a all-inclusive and common method for optimizing the DED process because many of the process parameters that interact are involved. [2].

1.2 Research objective

This study aims to analyze key parameters of the DED process on the single-track level, whereas previous studies typically used bulk models to directly investigate the effects of process parameters on final products. Grounded on the fact that a printed product is the aggregated single tracks, the effect on width, height and relative density of the printed part is collected by input process parameters (laser power, powder feed rate and coaxial gas rate) on a divided scale across single track, multi-track and multi-layer. All specimens are printed on the fixed experimental setting of the DED machine (i.e., MX-600) of which powder and substrate are SUS316L. The significance of the input process parameters is statistically analyzed on the key output of each scale. Then, the optimal parameters for the final product are compared to the parameters derived by the bulk samples.

1.3 Outline

In this study, optimizations are performed in such a way as to increase dimension sequentially and limit uncertainty, and optimizations are compared with another optimization method using cube specimens

The thesis consists of four chapters in total. A brief description of the background and the purpose of this thesis are already presented in Chapter 1. In Chapter 2, the related literatures will be introduced. Chapter 3 describes the experimental setup and provides analysis of the results about effects of process parameters on dimensional accuracy and relative density in DED with SUS316L powders. Chapter 5 presents the conclusion and describes future work.

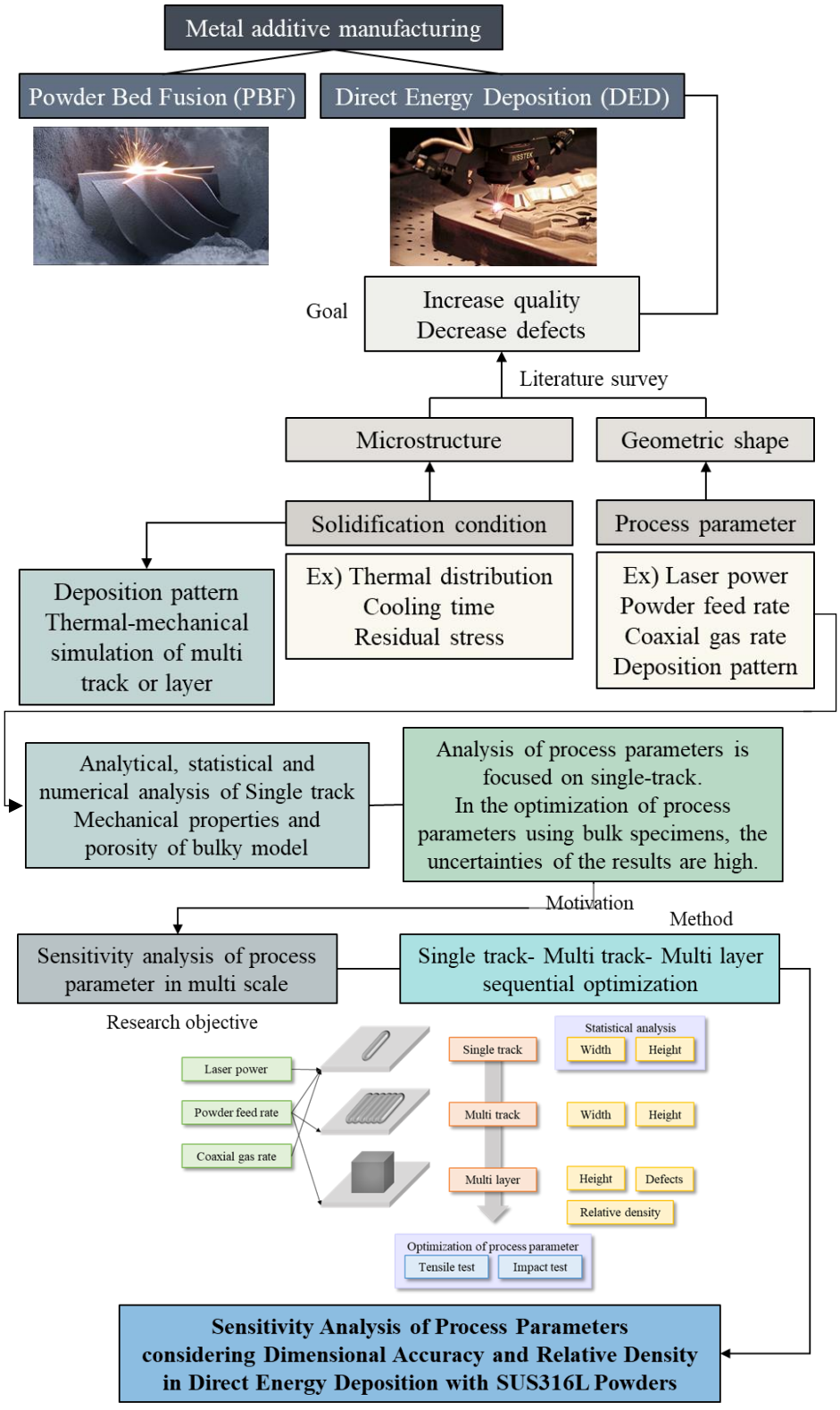

Figure 1.1 Outline

2. Literature Review

2.1 The Process of AM

The AM process is shown in Table 2.1 [3]. Firstly, in the pre-processing stage, a CAD model is created and then converted into a STL file. The STL format is a format developed by 3D Systems Inc in 1989, which consists of a solid model with triangular faces [4]. And then the STL file must be transferred to the AM machine. The next step is machine setup, which include slicing operation, support structure, and AM printer parameter setting. Then, 3D printed sample are built up and made.

After fabricating, post processing is needed. Post processing include support material removal, surface texture improvement, aesthetic improvement, and property enhancement using non-thermal or thermal techniques. Many 3D printers require support structure, and the process of removal them is required. The printed surface is rough include remnants of support, so heat treatment is used to adjust the strength, and Computerized Numerical Control (CNC) is used to fit tolerance.

Finally, the results should be measured using CMM or 3D scanner to validate the results before they can be used in the industry. Also, internal defects should be verified through non-parasitic inspection. After this verification process, it may be necessary to be assembled with other mechanical components to form the final product.

Table 2.1 AM process

	Step
1	CAD
2	Conversion to stereolithography (STL)
3	Transfer STL file to AM machine
4	Machine setup
5	Build
6	Removal
7	Post- processing
8	Application

2.2 The classification of AM

There are many ways to classify AM technologies. A common classification is based on technologies, like whether the machine uses lasers, extrusion, etc. [5]. The American Society for Testing and Materials has standardized and classified AM into seven categories: 1) Vat photopolymer, 2) material extrusion, 3) powder bed fusion, 4) direct energy deposition, 5) sheet lamination, 6) material jetting, 7) binder jetting [6].

Vat photopolymerization

Photopolymerization processes have been adopted to harden materials such as radiation-curable resins, liquid, or photopolymers [6]. There are many applications of photopolymer including coating ad printing industry and dentistry. These applications changed with Stereo Lithography Apparatus (SLA) in additive manufacturing. In this process, the build platform is submerged in liquid photopolymer, and the surface polymer is cured using a UV laser to create layers.

Material extrusion

Material extrusion process can be visualized similarly to cake icing. When pressure is applied, the material contained is ejected through the nozzle. If the pressure remains constant, the extruded material will flow at a constant rate and the cross-section diameter will remain constant. This diameter remains constant when nozzle is also maintaining at a constant speed that corresponds to the flow rate. The extruded material must be in the semi-solid state as it exits the nozzle. This material must be retained in its shape and fully hardened. In addition, materials must be bonded to the extruded material before a rigid structure can be constructed.

Sheet lamination

One of the additive manufacturing methods used primarily in the early stages of AM was Laminate Object Manufacturing (LOM). LOM is the way in which laser-cut paper material sheets become layers, and each layer represents a sectional layer of the CAD model of the part. The construction principle only cuts the appearance of the part, and the sheets can be cut by cutting, piling, or piling. These processes can be further classified according to interlayer joining mechanisms, such as adhesive or adhesive bonding, heat bonding, clamping and ultrasonic welding.

Table 2.2 The classification of additive manufacturing

Categories	Definition	Processes
Vat photopolymerization	"an additive manufacturing process in which liquid photopolymer in a vat is selectively cured by light- activated polymerization"	Stereo Lithography Apparatus (SLA); Digital Light Processing (DLP)
Material extrusion	"an additive manufacturing process in which material is selectively dispensed through a nozzle or orifice"	Fused Filament Fabrication (FFF);
Powder bed fusion	"an additive manufacturing process in which thermal energy selectively fuses regions of a powder bed"	Selective Laser Sintering (SLS); Selective Laser Melting (SLM); Electron Beam Melting (EBM)
Direct energy deposition	"an additive manufacturing process in which focused thermal energy is used fuse materials by melting as they are being deposited"	Direct Metal Deposition (DMD)
Sheet lamination	"an additive manufacturing process in which sheets of material are bonded to form a part"	Laminated Object Manufacturing (LOM)
Material jetting	"an additive manufacturing process in which droplets of build material are selectively deposited"	Polyjet; Multi Jetting Modeling (MJM)
Binder jetting	"an additive manufacturing process in which a liquid bonding agent is selectively deposited to join powder materials"	3 Dimensional Printing (3DP)

Material jetting

In material jetting (MJ), all the part material is distributed from a print head. This contrasts with binder jetting, where binder or other additive is printed onto a powder bed which forms the bulk of the part. A material jetting process are created that relate pressure needed to fluid properties.

Binder jetting

Binder jetting, which is called the 3D Printing (3DP) process, was developed by MIT in the early 1990s. A binder is selectively deposited in the powder bed, and these areas are joined. Materials generally used in binder jetting are metal, sand, and ceramics in fine form. Binder-jetting is used for a variety of applications, including full-color prototypes, large sand-casting cores, and molds.

Powder bed fusion

The term powder bed fusion is defined as an additive manufacturing process in which thermal energy selectively fuses regions of a powder bed [6]. A lot of attention has been paid to the metal AM method recently, of which PBF 3d printing is most commonly used. Materials used in PBF include aluminum, titanium and iron. The PBF process uses a high-power laser that melts metal powder to create each layer, as shown in Figure 2.1. Because the PBF uses metal, it is difficult to process it as a thermal strain and requires a support structure, resulting in a dross formation on the surface of the protrusion when built without a support structure. Support structures are used to mitigate this dross formation [7].

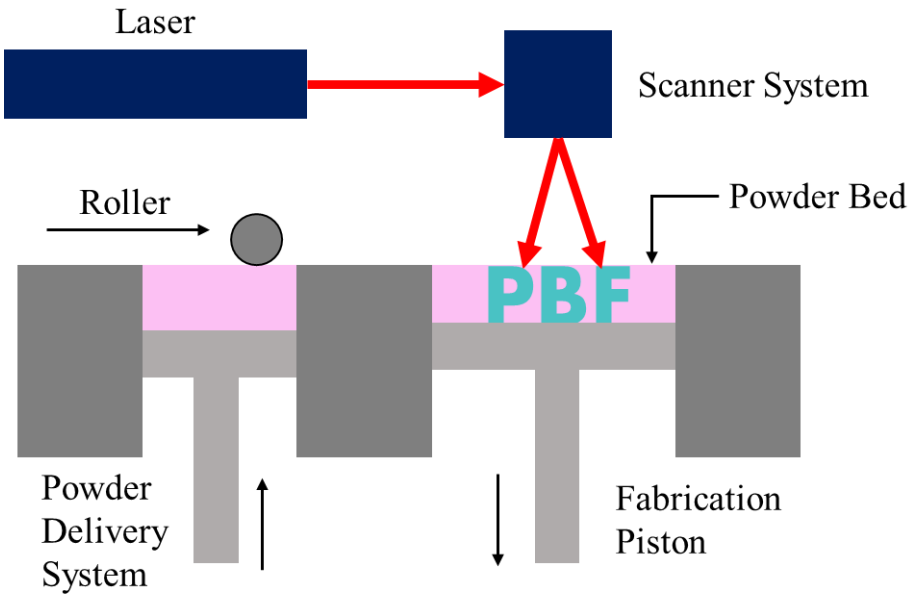

Figure 2.1 The schematic of Powder Bed Fusion

The PBF has high dimensional accuracy and is made of furnaces, so it has excellent material properties and high density. However, as described above, production requires a support structure, and therefore requires work and tools to remove the support structure. [8].

Direct energy deposition

The term direct energy deposition is defined as "an additive manufacturing process in which focused thermal energy is used to fuse materials by melting as they are being deposited" [6]. DED is a way to create metal parts like PBF. However, without separate material and selective energy transfer, DED combine material/energy transfer for deposition and part formation simultaneously within similar areas as shown in Figure 2.2. Metal preforms can be wires or powders, the latter being supported by much richer and more modern DED machines. Wire feed DEDs provide more control over deposition efficiency, while powder preforms generally occur through nozzles and may accumulate unused powder on the DED machine. The previous DED system consisted of a single coaxial nozzle (coaxial to laser beam) in the atmosphere, and today the DED machine has up to four nozzles and can use inert gas to minimize the high oxidation rate inherent in high temperature metal processing. [9].

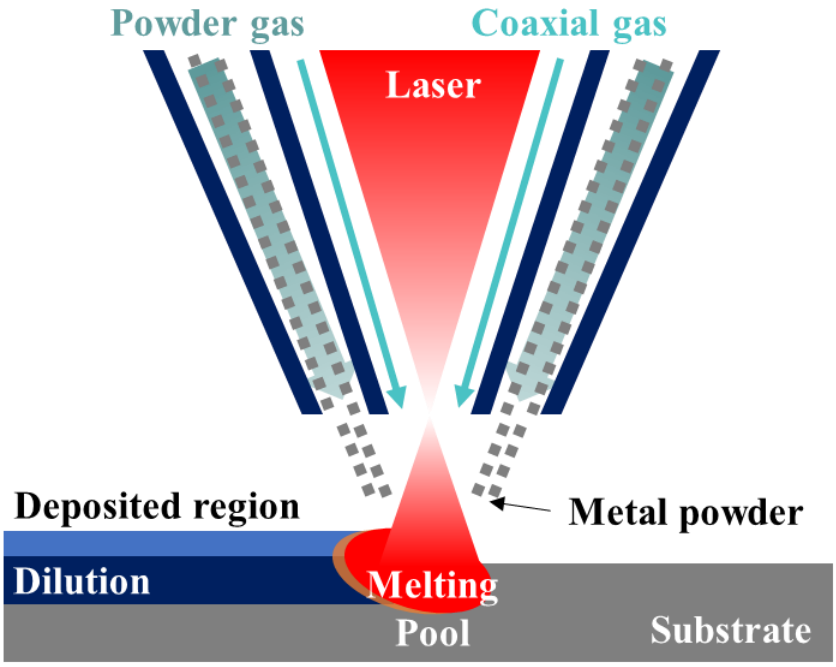

Figure 2.2The schematic of Direct Energy Deposition

The main difference between PBF and DED is that they can leverage the needs of a variety of applications and end users. PBF process provides better surface quality in final parts than DED process. However, PBF process needs the procedure of removing support structure. PBF process has the advantage to a complex part since powder bed plays a role of support. PBF uses smaller powder than DED, so the laser used in PBF has lower power. DED do not rely on pre-leak layers

of metal powder and can be used to repair or coat parts through cladding. In addition, the multi-material/energy transfer method makes it easy to use DED to create functional grade/composite parts with varying material/alloy concentrations. Finally, DED, such as coaxial powder supply and lateral wire supply, allow for pre-form blending. [9].

Although PBF shares much of the origin of plastic prototyping technology, DED shares many process characteristics with laser-welded sheathing and five-axis laser welding in many ways. DED software can be more complex than PBF or laser sheaths when relying on functional-based model and CNC tool path control than when strictly dependent on flat-panel slicing of STL models. A substrate plate or part is required to start deposition. The substrate may or may not be part of the final part. Hybrid applications may require a DED to add functionality to existing base components or to the shape of commercial feedstock. The DED can store materials on complex 3D surfaces that move the joints of both the laser deposition head and substrate parts simultaneously by more than five axes (except simple plane and X and Y movements). [10]

Important process parameters include track scan interval, powder feed rate, beam pass rate, beam output and beam spot size. Powder feed rates, beam power and pass rates are all interrelated. For example, increasing the supply speed has a similar effect as decreasing the beam output. Similarly, increasing the beam power or powder supply speed and decreasing the speed of passage both increases the sedimentation thickness. From the energy point of view, increasing scan speed is a short dwell time, which reduces input beam energy, resulting in a smaller melt pool in the substrate and faster cooling [11].

Scanning patterns also play an essential role in part quality. As mentioned earlier, it may be desirable to change the direction of the scan from layer to layer to minimize residual stress growth. The track width hatch interval must be set to overlap adjacent beads, and the layer thickness setting must be less than the depth of the melt pool to create a product that is fully dense. Sophisticated accessory equipment for melt pool imaging and real-time sediment height measurements to accurately monitor the properties of melt pool and melt pool are additional values for repeatability, as the size, shape and temperature of the melt pool can be used as the feedback control input to maintain the desired pool characteristics. To control the sedimentation thickness, the movement speed can be dynamically changed according to sensor feedback. Similarly, in order to control the solidification speed and thus control microstructure and properties, the melting pool size can be dynamically changed to monitor and control. [11].

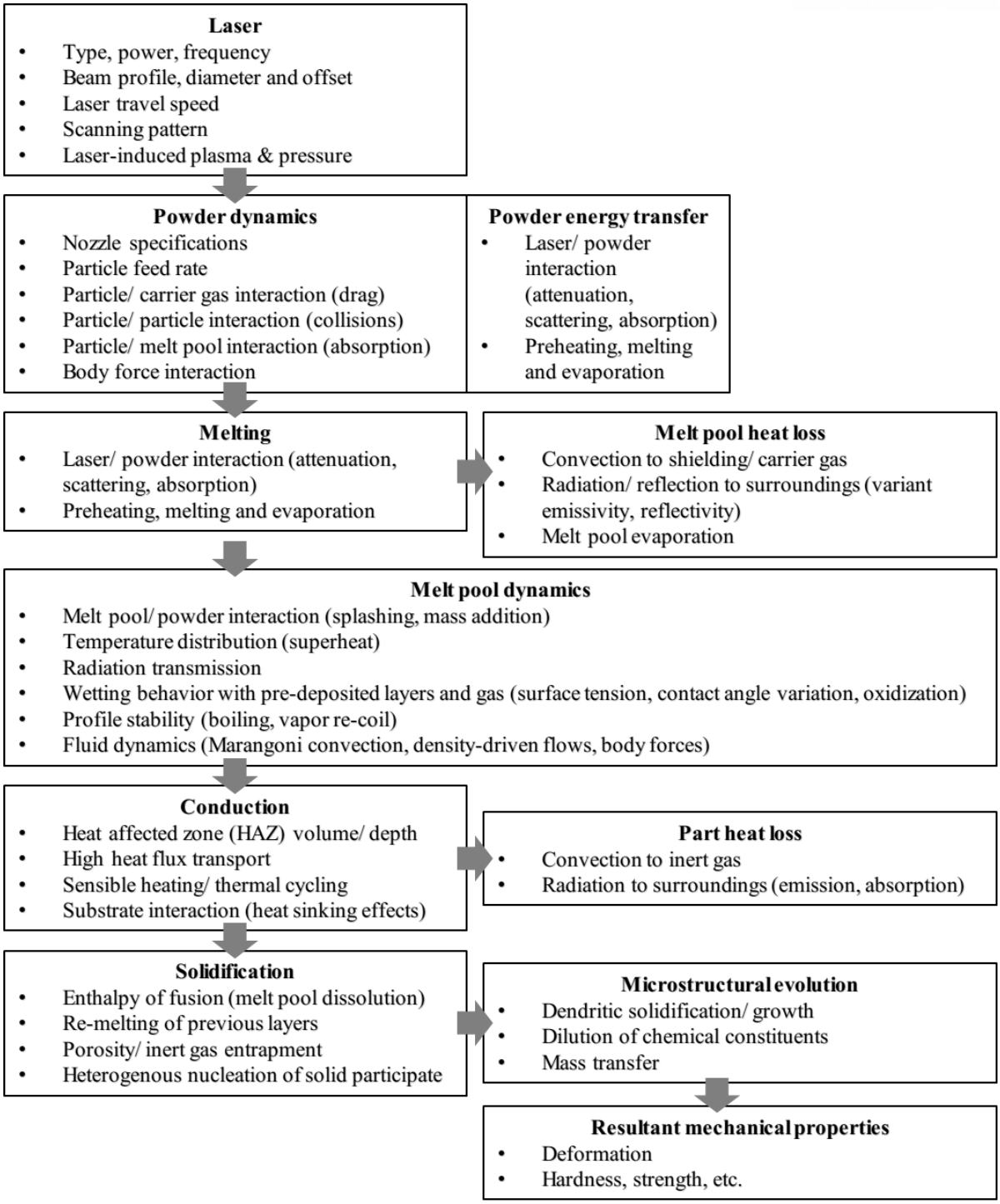

Figure 2.3 Physical events occurring in DED process

2.3 Defects in DED

When injecting excess powder into the melt pool, excess dissolved powder particles adhere to the cladding surface. Powder efficiency is relatively low because the energy supplied cannot completely dissolve the powder. This occurs in cladding with high speed and low speed laser power. This type of fault occurs due to an unbalanced mass energy supply.

Process optimization based on powder efficiency is required. To melt excessive powder particles, laser output should be increased. To reduce the attenuation of the laser beam, the speed of the powder supply shall be reduced. The attenuation of laser power depends on the size of the particle, the flight speed of the particle, and the powder supply speed. Other supply structures (coaxial nozzles and off-axis nozzles) affect the laser power density reaching the substrate surface. Because the size of the melt pool depends on the laser energy reaching the substrate, this need to be considered when adjusting the powder supply rate. The mass energy balance between laser light and powder stream/cloud can be met by adjusting both laser power and powder supply speed. In addition, the impact of un-melted powder particles can interfere with the melt pool. Melt pool can lead to porosity of shielding or carrier gas during rapid solidification because excessive powder particles do not melt when they reach the melt pool.

Multiple longitudinal and transversal cracks in clad layer are shown in Figure 2.4. The longitudinal crack initially starts from the start/ end position. It has propagated along the cladding direction between the clad tracks where the valley (undercut) is formed. The undercut formation between clad tracks promotes longitudinal cracking. This type of cracking further develops transversal cracks as shown in Figure 2.4. Transversal cracking across the clad tracks is due to high stresses along the cladding direction which result from thermal mismatch and the rapid cooling process. The longitudinal cracking can be eliminated by a laser power ramping program at the start or stop position and by having a large overlap ratio (40 to 50%) whereby the undercut formation is avoided. The transversal cracking can be avoided by optimizing the thermal cycles. However, the material properties (hardness and ductility) also contributes to transversal cracking. The transversal cracking can be avoided by preheating the substrate when crack sensitive materials are used. Figure 2.4 shows examples of porosity appearing in the clad layer. It is difficult to avoid the porosity since the powder is delivered into the melt pool by an inert gas. Larger porosity is generated under poor cladding conditions. However, the size and number of the porosity can be reduced by controlling the process conditions. Figure 2.4 a shows large porosity appearing in the clad layer. The clad layer was produced with 1,000 W of laser power, 13.3 mm/s of cladding speed and 0.139 g mm/s of powder feeding rate. Figure 2.4 shows small porosity appearing in the clad layer. The clad layer was produced with 1,000 W of laser power, 13.3 mm mm/s of cladding speed

and 0.111 g mm/s of powder feeding rate. The average size of the pores reduces from around 200 μm to 50 μm. In most cases, fine pores do not contribute to crack nucleation or growth as the larger ones do. This is also the case with welding of metals [12].

It is well known that the relative density has a positive relationship with forming quality because it could reflect the cracks and pores inside the parts [13] It indicated that though the sample density increased with the increase of laser power, the scanning speed had the most significant negative effects on the density change. However, the changes of the powder flow rate did not have obvious impacts.

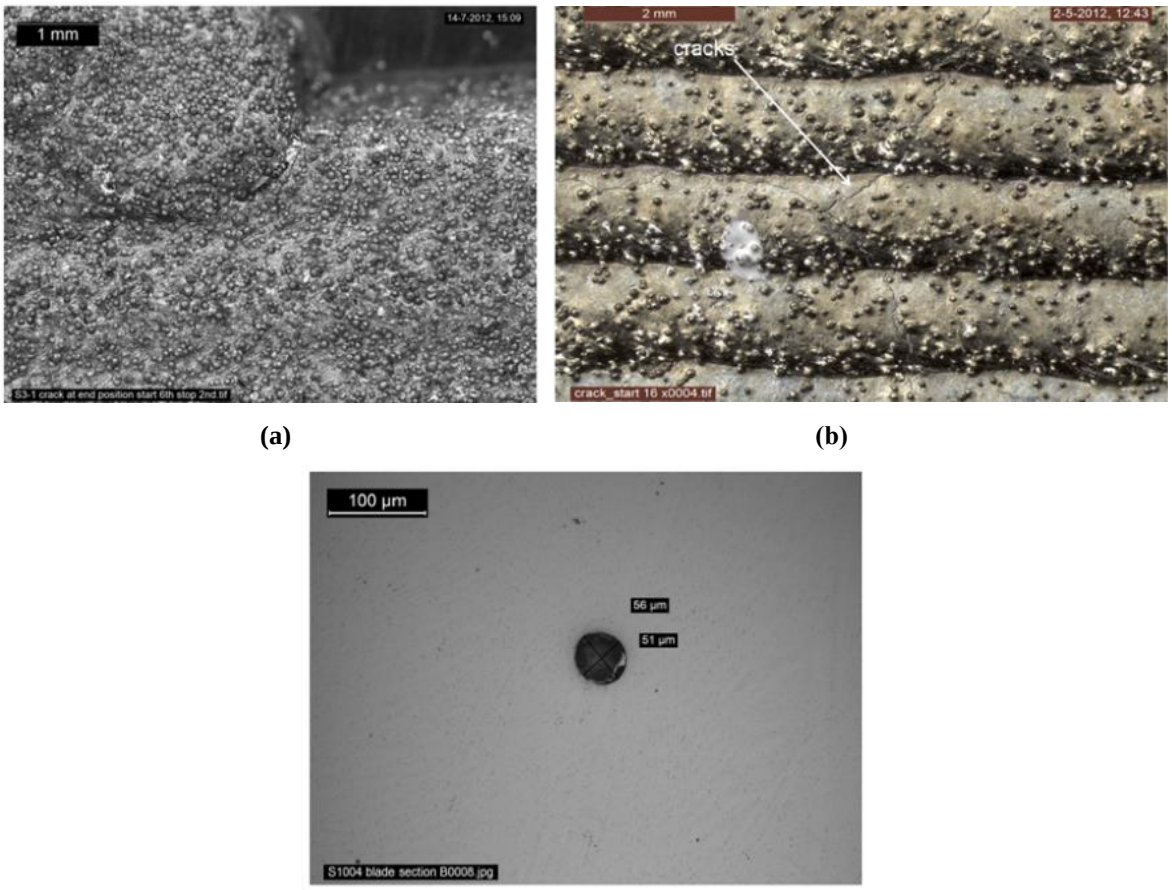

(a) **(b)**

(c)

Figure 2.4 Defects in DED, (a) Example of excessive unmelt powder particles, (b) Example of cracks (c) Porosity

2.4 Process parameters study in DED

2.4.1 Single track

There are many analyses of laser cladding, which is almost same with single track in DED. In order to predict a geometry of single-track cross section, researchers have made many attempts.

Table 2.3 Various research about single track cross section

	Material	Substrate	Process parameter	Section properties	Note
[14,15]	SUS316L	Low steel carbon	Laser power, powder feed rate, scanning speed	Width, Height	Compare the regression model made from the section properties with the analytical equation
[16]	SUS316L	Low steel carbon	Scanning speed, hatching space	Height	the regression model made from the section properties and analysis of microstructure and micro hardness
[17]	SUS316L	S45C	powder size, powder dispensing method scanning speed	Height, dilution	Presenting appropriate powder conditions through section properties and surface quality
[18]	SUS316L , IN718	S45C	Laser power, powder feed rate, coaxial gas rate	Height, dilution	Analysis of tendency according to process parameters through section properties and surface quality
[19]	IN718	Mild steel(S235JR)	Laser power, powder feed rate, scanning speed	Width, height, α(clad angle)	Process map production through regression analysis

Cheikh et al. [14, 15] reported analytical relationship between the singlet tracks geometrical characteristics (height, width, dilution depth, area) and the process parameters (laser power, scanning speed, powder feed rate). This researched two kind of model for predicting geometric characteristics of single-track cross section. The first one is analytical model governed by powder distribution. three powder distributions are proposed: Gaussian, uniform, polynomial. The second model is about cross section which is supposed to be a disk shape since the surface tension forces. The radius and the center of the disk are determined by process parameters.

Following [14, 15] Cheikh et al. researched about thin walls made with different velocities and different hatching space. 1, 3, 5, and 10 layers walls are analyzed, and finding optimal construction [16]. A relationship between the process parameters and the wall height is achieved with correlation.

2.4.2 Bulk model

Beyond the analysis of process parameters in single track, various studies are also being conducted on bulk models made through the DED process. Tests were conducted primarily on mechanical properties such as tensile testing, impact testing, and microhardness [20-27]. Some studies are also being conducted to decrease residual stress by preventing concentration of energy using the deposition pattern [27-31].

2.4.3 Process parameter study using SUS316L

SUS316L material has high-temperature strength and corrosion resistance of the internal system under welding conditions with ultra-low carbon steel. Therefore, SUS316L has been widely used as a welding metal powder. Because the DED process is also similar to welding, SUS316L is commonly used by various industry groups. Process parameter study using SUS316L is organized in Table 2.4. As shown in the Table 2.4, it is necessary to optimize process parameters by machine or material to use the DED process for reasons such as the use of different types of laser by machine.

Table 2.4 Process parameter study using SUS16L

	Year	**Powder**	**Process parameter**			
		size	Laser power [W]	Scan speed [mm/s]	Powder feed rate [g/min]	Coaxial gas rate [l/min]
[32]	2018		500-2500	1-10	15-30	15
[22]	2017		150, 200, 250	8.5, 12.7, 17	7, 10, 13.5	
[33]	2019		700-900	650-1050	≥6.5	4-6
[18]	2017	45-150	500, 700, 900		3, 6, 9	2, 4, 6, 8
[14]	2011	45-75	180, 280, 360	300, 600, 900	1.5, 3, 4.5	
[27]	2019	25-53	34.3, 45.3	0.4, 0,5, 0.6	3.09, 2.81, 2.46	
[24]	2018		470, 478, 645	2-19	0.9-28.8	

3. Sensitivity analysis of process parameters

To improve quality and reduce defects in direct energy deposition process, effects on geometric shape of process parameters are analyzed. Using the result, process parameters are optimized with SUS316L. In this section, the sensitivity analysis of process parameters was conducted through analysis at multi scales and sequential optimization in order to overcome anal that analysis of process parameters performed only on single track and the lack of detailed analysis of input parameters in the optimization process parameter using bulk models. In section 3.1, a total of 27 cube specimens of three levels were produced from three parameters (laser power, powder supply and gas supply), analyzed the height and relative density, and then derived the optimal process parameter value using the response optimization tool. In section 3.2, the width, height and relative density were then analyzed by producing 216 single track specimens of 6 level, 11 multi-track specimens, and 4 multi-layer (=cube) specimens with the three parameters using a multi-scale specimen. Based on the results of the analysis, the optimal process parameter values are also derived, compared to the optimal process parameter extracted earlier, and verified through mechanical properties test.

3.1 Sensitivity analysis using cube specimens

3.1.1 Experimental setup

MX-600 (Insstek) in figure 3.1 is used for using DED process. All kind of Powder type metals can be printed, and dissimilar material bonding is possible. It is often used for repair of existing break molds. Maximum buildable size is 450×600×350mm.

Figure 3.1 Machine of direct energy deposition (MX- 600)

The powder was made of a material of 45 to 150 um size SUS316L. SUS316L material was used to identify laminated surface and section characteristics according to process parameters because of its high temperature strength and corrosion resistance of the internal system under welding conditions with ultra-low carbon steel. The composition of SUS316L was as follows and the XRF analysis was performed to understand the correct composition. Table 3.1 is XRF analysis result of SUS316L powder

Table 3.1 XRF analysis of SUS316L powder (%)

Element	Fe	Cr	Ni	Mo	Mn	Si	Cl	Cu
Content	63.91	17.09	13.78	3.552	1.332	0.203	0.0459	0.04

Process parameters were designed at 3 levels for three factors: Powder feed rate, laser power and coaxial gas rate. values of the parameters are used as shown in Table 3.2. Cubes (15×15×15 mm) are printed at SUS316L substrate (100×100×15 mm) as shown in Figure 3.2. The printed specimens were cut with wire-cutting, then micro-polished the cross-section, then measured Z-direction height and relative density using a metal microscope. The main effects of the results were then analyzed using Minitab.

Table 3.2 Value of process parameters

Laser power[W]	Powder feed rate[g/min]	Coaxial gas rate[l/min]
300	4.5	6.5
350	5.0	7
400	5.5	7.5

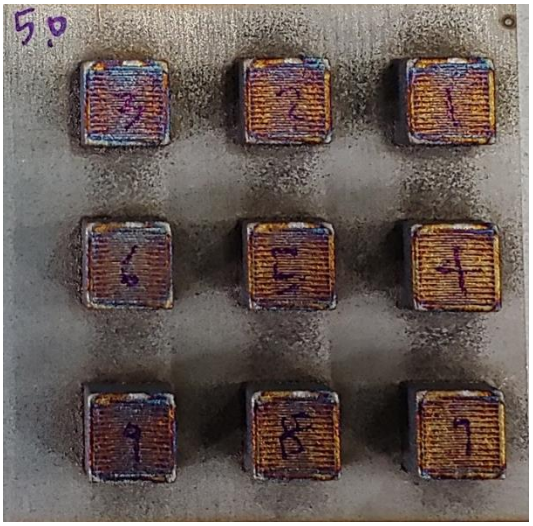

Figure 3.2 Example of cube specimen

3.1.2 Results

In the case of the height(Z), the ANOVA results is shown by Table 3.3. The CAD data value of height is 15mm. As a result, the parameters Powder Feed Rate (PFR), Laser Power (LP), Coaxial Gas Rate (CGR), and interactions were all significant. The factor with the most significant effect is the powder feed rate. In addition, the regression analysis results in Equation 3.1, a regression equation for Z. The R-square value of the regression equation is 83.53%.

(Equation 3.1) $$Z = -79.7 + 18.48PFR + 0.257LP + 13.12\ \text{CGR} - 0.0500\ \text{PFR} \times \text{LP} - 2.55\ \text{PFR} \times \text{CGR} - 0.0365\ \text{LP} \times \text{CGR} + 0.00710\ \text{PFR} \times \text{LP} \times \text{CGR}$$

First, outlier data were checked through the histogram of the residuals. The normal probability plot of the residuals confirmed the assumption that the residuals are normally distributed. In addition, the residuals versus fits plot confirmed the assumption that there is a constant variance in the residuals, and the residuals versus data order plot confirmed the assumptions that the residuals are not related to each other as shown in Figure 3.3.

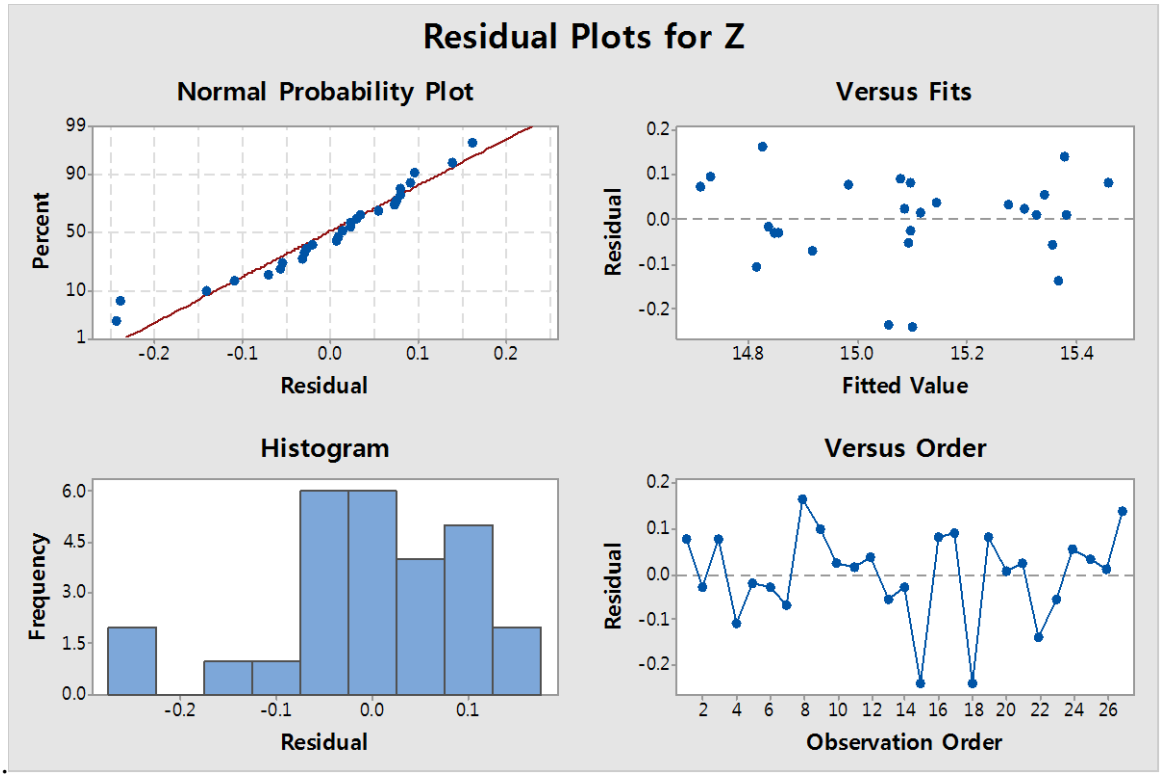

Figure 3.3 Residual plots for height(Z)

In the case of the Relative density (RD), the ANOVA results is shown by Table 3.4. As a result, all parameters are not significant about the relative density. However, relative density is greater than 99.95% for all treatment in the experiment space. It is acceptable when the product is manufactured using typical metal manufacturing process. Therefore, DED process seems to be a competitive tool for relative density. The result of response optimization using the Equation 3.1 about height is shown in Figure 3.5 powder feed rate 4.8566g/min, laser power 300W, coaxial gas rate 6.5l/min.

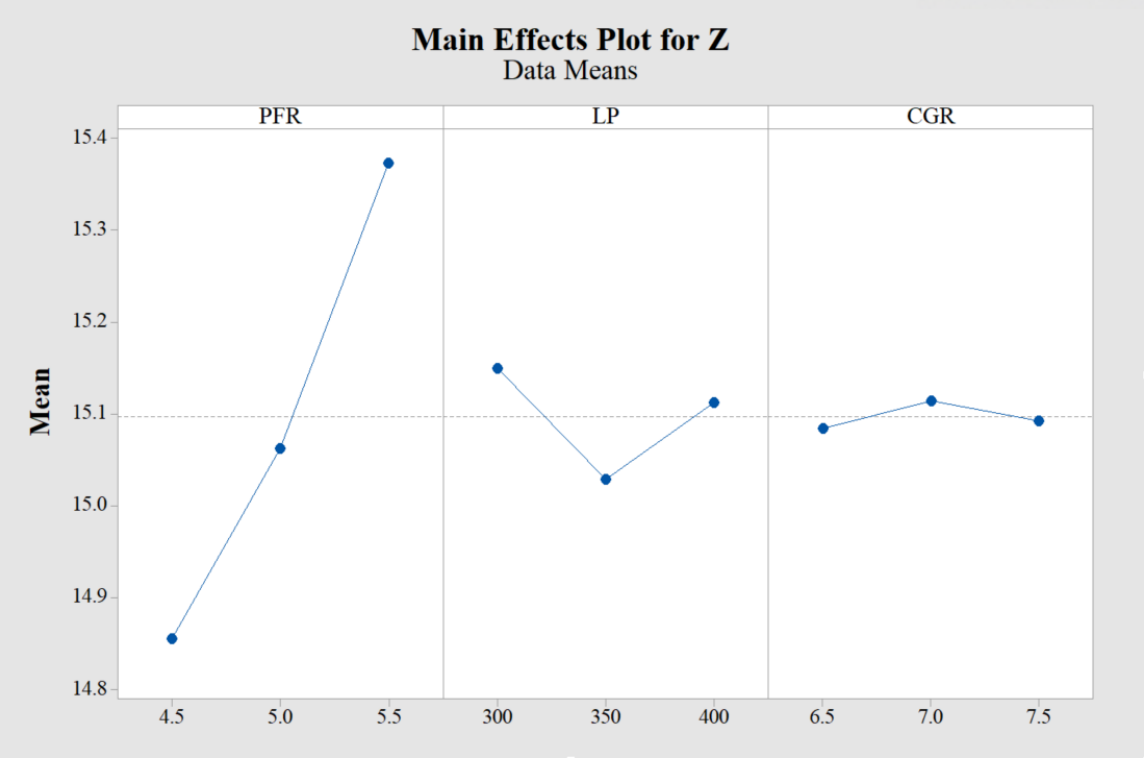

Figure 3.4 Main effect plot for height

Table 3.3 ANOVA for height

	DF	Adj SS	Adj MS	F-value	P-value
PFR	1	0.06996	0.06996	5.23	0.034
LP	1	0.06653	0.06653	4.98	0.038
CGR	1	0.06882	0.06882	5.15	0.035
PFR*LP	1	0.06356	0.06356	4.76	0.042
PFR*CGR	1	0.06555	0.06555	4.90	0.039
LP*CGR	1	0.06617	0.06617	4.95	0.038
PFR*LP*CFGR	1	0.06301	0.06301	4.71	0.043
Error	19	0.25393	0.01336		
Total	26	1.54156			

S	R-sq	Adj R-sq	Predicted R-sq
0.115605	83.53%	77.46%	60.80%

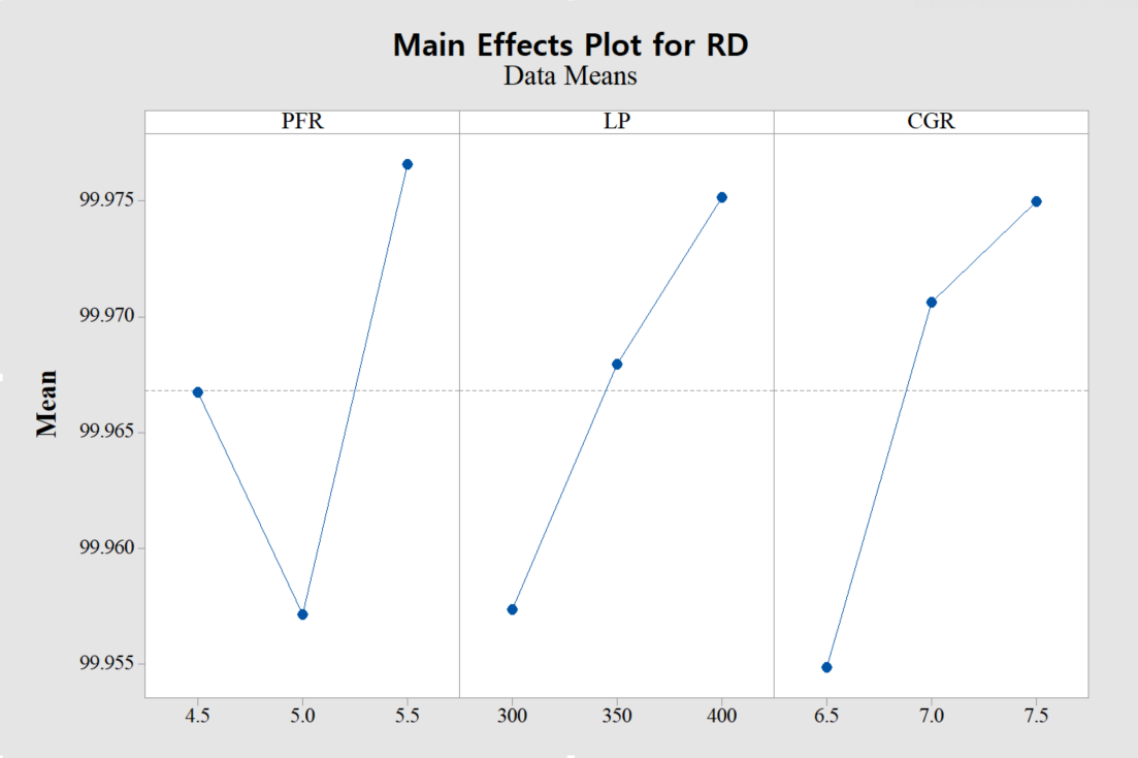

Figure 3.5 Main effect plot for relative density

Table 3.4 ANOVA for relative density

	DF	Adj SS	Adj MS	F-value	P-value
PFR	1	0.000480	0.000480	0.96	0.339
LP	1	0.000443	0.000443	0.89	0.358
CGR	1	0.000411	0.000411	0.82	0.376
PFR*LP	1	0.000482	0.000482	0.96	0.339
PFR*CGR	1	0.000460	0.000460	0.92	0.349
LP*CGR	1	0.000427	0.000427	0.85	0.367
PFR*LP*CFGR	1	0.000459	0.000459	0.92	0.350
Error	19	0.009500	0.000500		
Total	26	0.013179			

S	R-sq	Adj R-sq	Predicted R-sq
0.0223602	27.92%	1.36%	0.00%

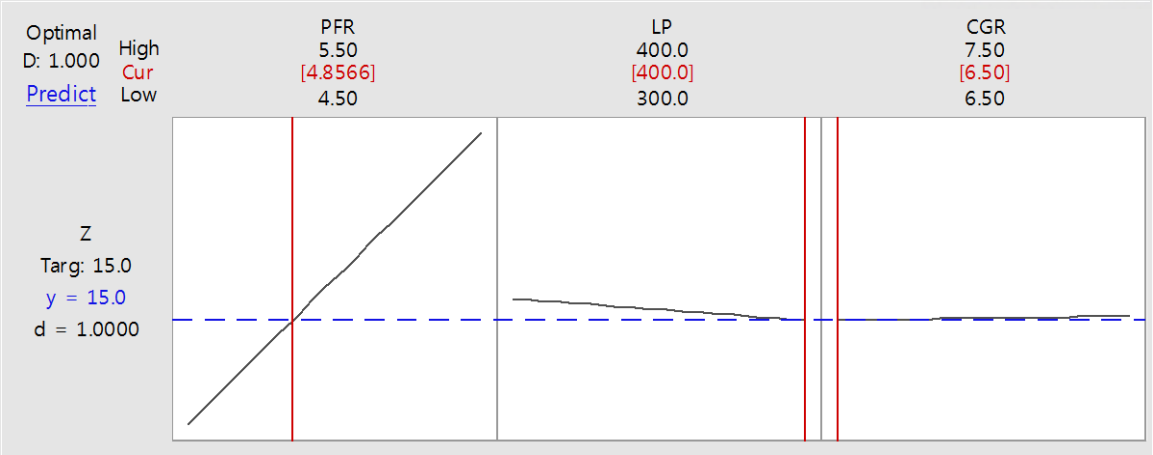

Figure 3.6 optimization plot of height

3.2 Sensitivity analysis in multi scale

3.2.1 Experimental Setup

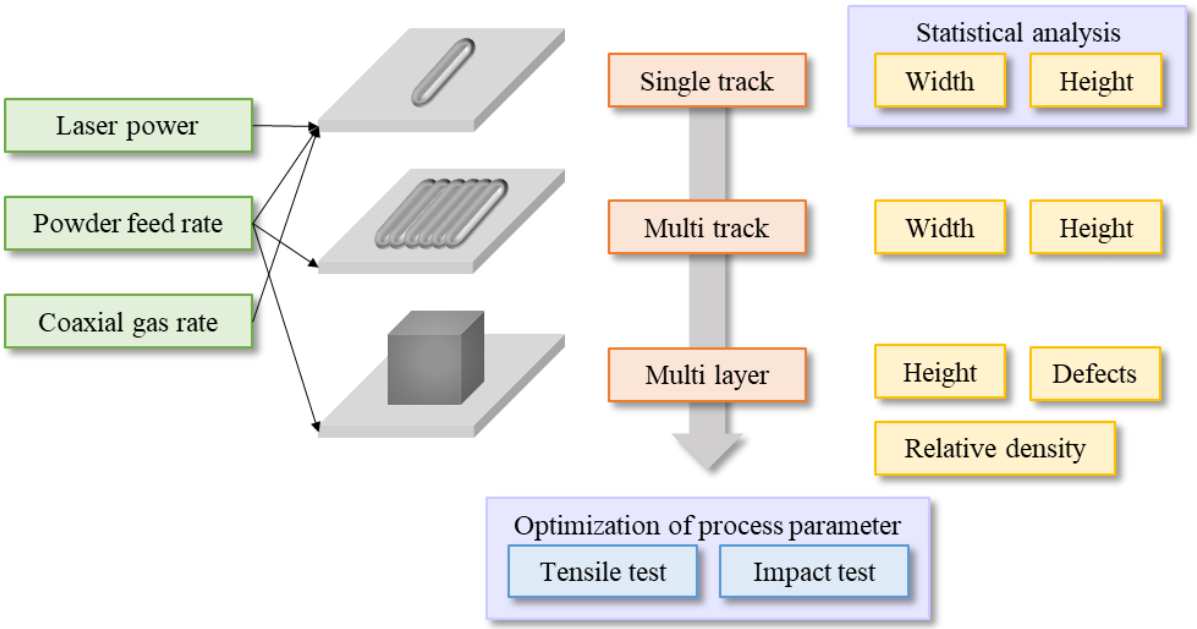

Figure 3.7 Flow chart of experiment

For equipment and materials, MX-600 equipment and SUS316L powder were used as described in Section 3.1. For the process parameters, the experimental design was performed at 6 levels for three factors: Powder feed rate, laser power, and coaxial gas rate. The value of process parameter is shown in Table 3.5. Width and height were measured by building 216 single tracks with a length of 10mm. The height and width of the 11 multi tracks were then measured, and the height and relative density were measured, and the defects were identified as shown in Figure 3.7.

Table 3.5 Value of process parameters

Laser power [W]	Powder feed rate [g/min]	Coaxial gas rate [l/min]
350	3.5	4
450	4.5	5
550	5.5	6
650	6.5	7
750	7.5	8
850	8.5	9

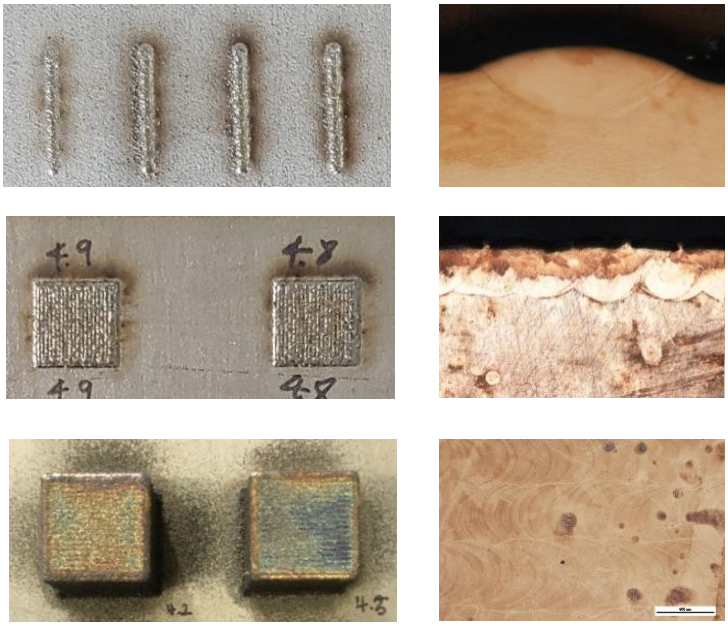

Figure 3.8 Actual deposited geometry and cross section

3.2.2 Sensitivity analysis of process parameters in single track

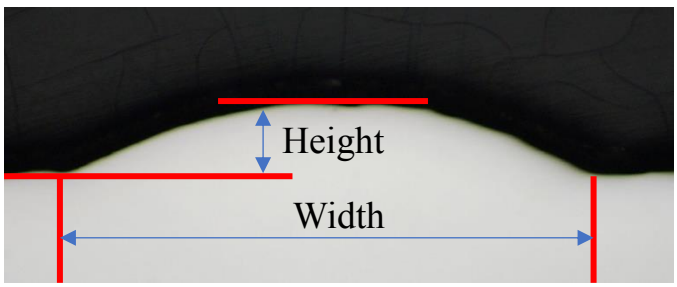

Figure 3.9 cross section of sing track

Main effects plot was performed for height and width of single track. In the case of the width, the ANOVA results is shown by Table 3.6. As a result, the parameters LP is significant. In the case

of the height the ANOVA results is shown in Table 3.7. As a result, the parameter PFR is significant

(Equation 3.2) Width = 0.4189 + 0.001681 LP + 0.0406 CGR - 0.000102 LP × CGR

(Equation 3.3) Height = 0.04163 + 0.02702 PFR - 0.000014 LP × PFR - 0.002613 PFR × CGR + 0.000006 LP × PFR × CGR

Based on significant results, the regression equation above 3.2 and 3.3 was derived from the rerun of the regression analysis. In this case, the R-square values for the width and height are 78.21% and 76.61%. As shown in Figure 3.11 and 3.13, outlier data were checked through the histogram of the residuals. The normal probability plot of the residuals confirmed the assumption that the residuals are normally distributed. In addition, the residuals versus fits plot confirmed the assumption that there is a constant variance in the residuals, and the residuals versus data order plot confirmed the assumptions that the residuals are not related to each other. Therefore, above regression model satisfied assumption and appropriate.

Due to the unit differences, the factor design was designed to increase by 100 for LPs and by 1 for PFRs and CGRs. Thus, when looking at the coefficients of regression equation, it appears that LP has a greater effect than CGR for width, and PFR for height has the greatest effect.

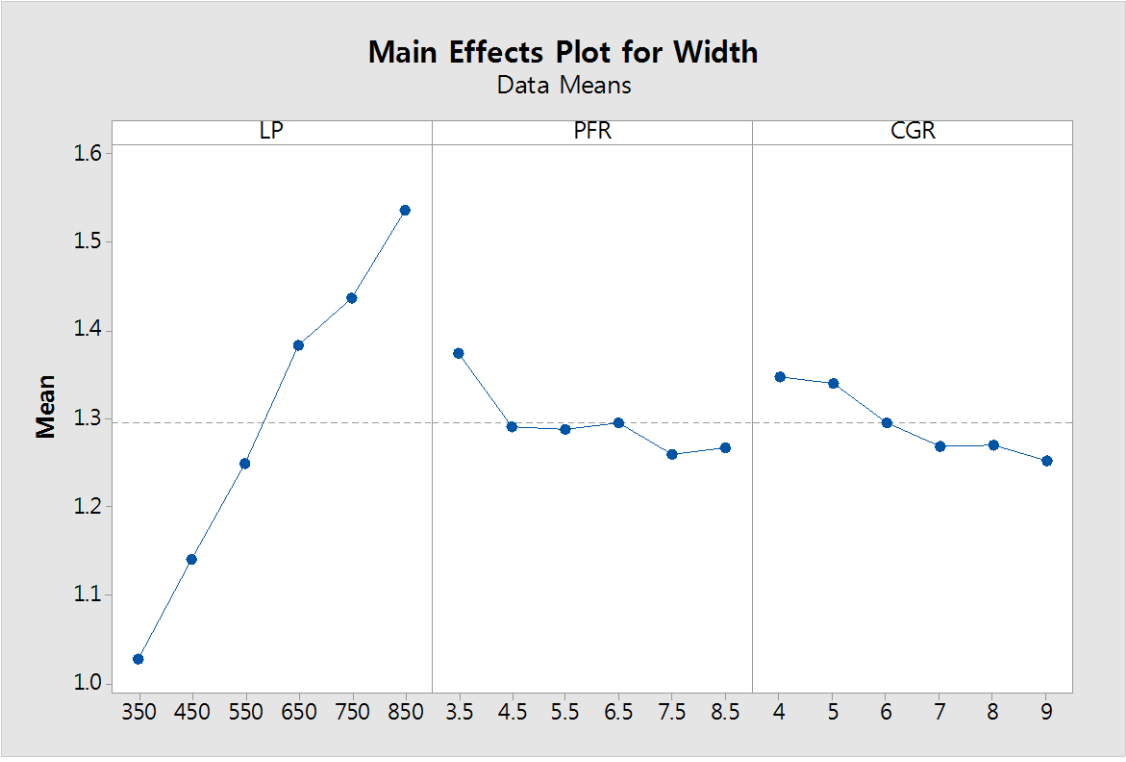

Figure 3.10 Main effect plot for width in single track

Table 3.6 ANOVA for width in single track

	DF	Adj SS	Adj MS	F-value	P-value
PFR	1	0.00402	0.00402	0.49	0.483
LP	**1**	**0.16373**	**0.16373**	**20.15**	**0.000**
CGR	**1**	**0.03458**	**0.03458**	**4.25**	**0.040**
PFR*LP	1	0.01335	0.01335	1.64	0.201
PFR*CGR	1	0.01296	0.01296	1.60	0.208
LP*CGR	**1**	**0.06256**	**0.06256**	**7.70**	**0.006**
PFR*LP*CFGR	1	0.01853	0.01853	2.28	0.133
Error	208	1.69049	0.00813		
Total	215	8.93175			

S	R-sq	Adj R-sq	Predicted R-sq
0.0901518	81.07%	80.44%	79.56%

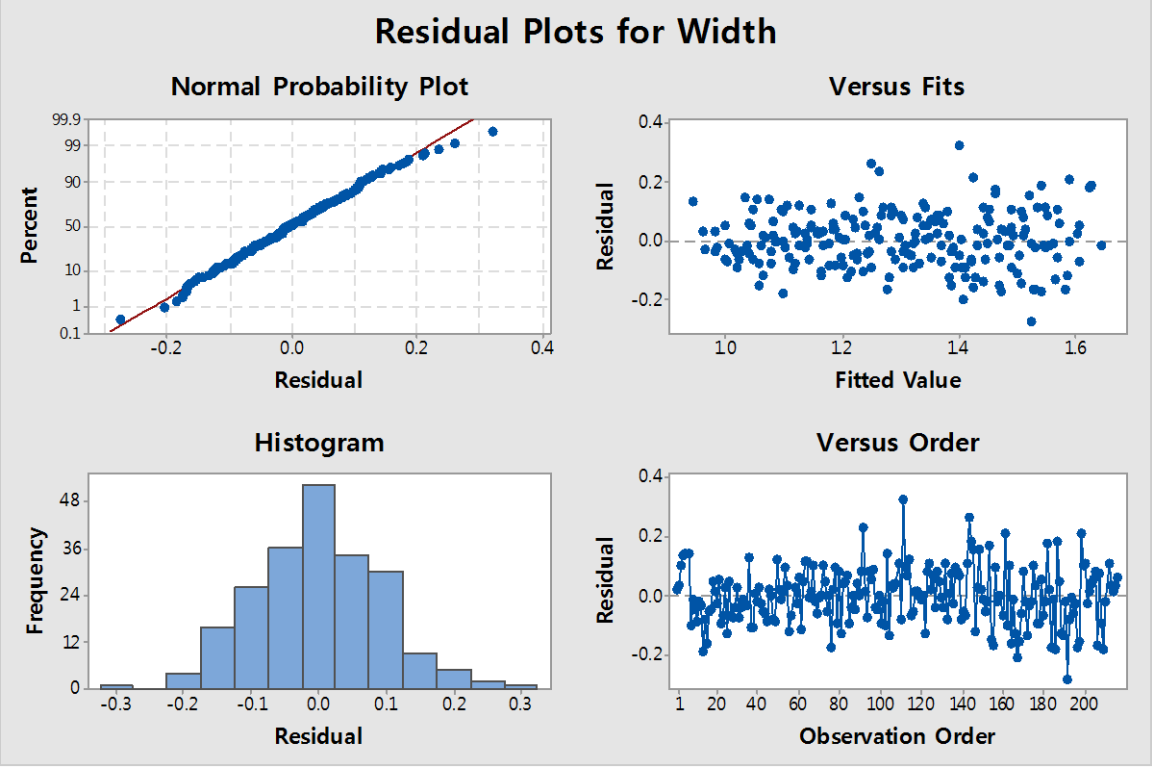

Figure 3.11 Residual plots for width

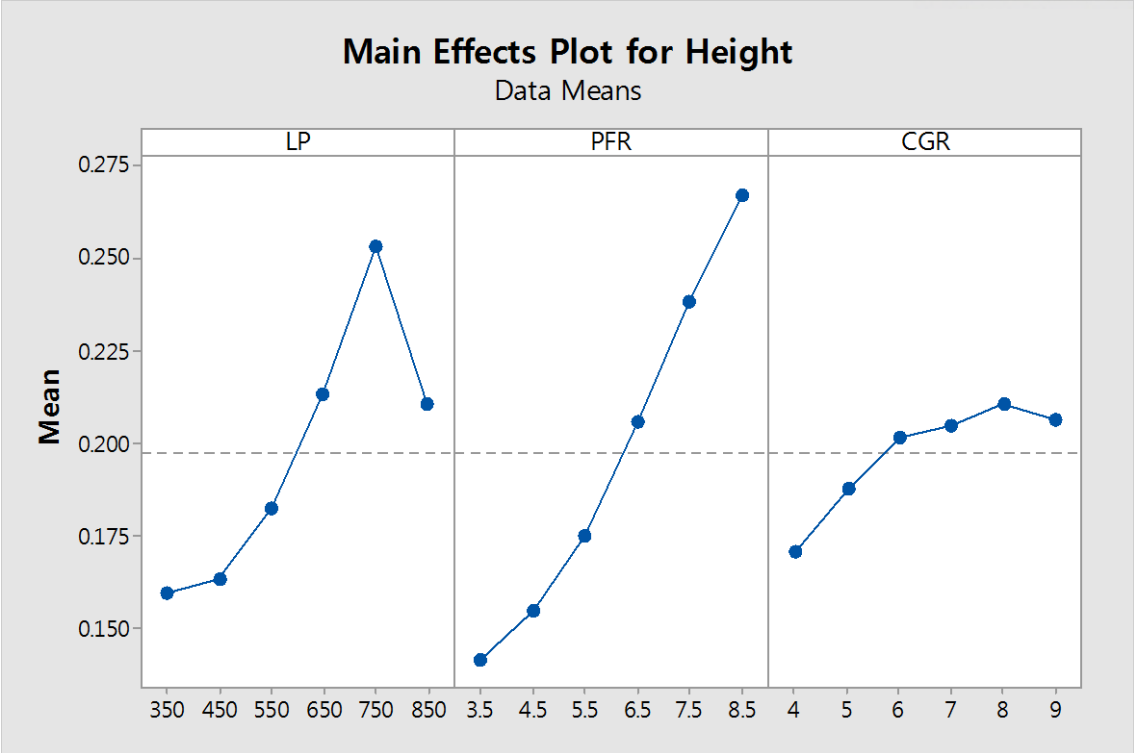

Figure 3.12 Main effect plot for height in single track

Table 3.7 ANOVA for height in single track

	DF	Adj SS	Adj MS	F-value	P-value
PFR	**1**	**0.009713**	**0.009713**	**10.51**	**0.001**
LP	1	0.002472	0.002472	2.68	0.103
CGR	1	0.003070	0.003070	3.32	0.070
PFR*LP	**1**	**0.004000**	**0.004000**	**4.33**	**0.039**
PFR*CGR	**1**	**0.007048**	**0.007048**	**7.63**	**0.006**
LP*CGR	1	0.002661	0.002661	2.88	0.091
PFR*LP*CFGR	**1**	**0.009102**	**0.009102**	**9.85**	**0.002**
Error	208	0.192141	0.000924		
Total	215	0.850693			

S	R-sq	Adj R-sq	Predicted R-sq
0.0303933	77.41%	76.65%	75.36%

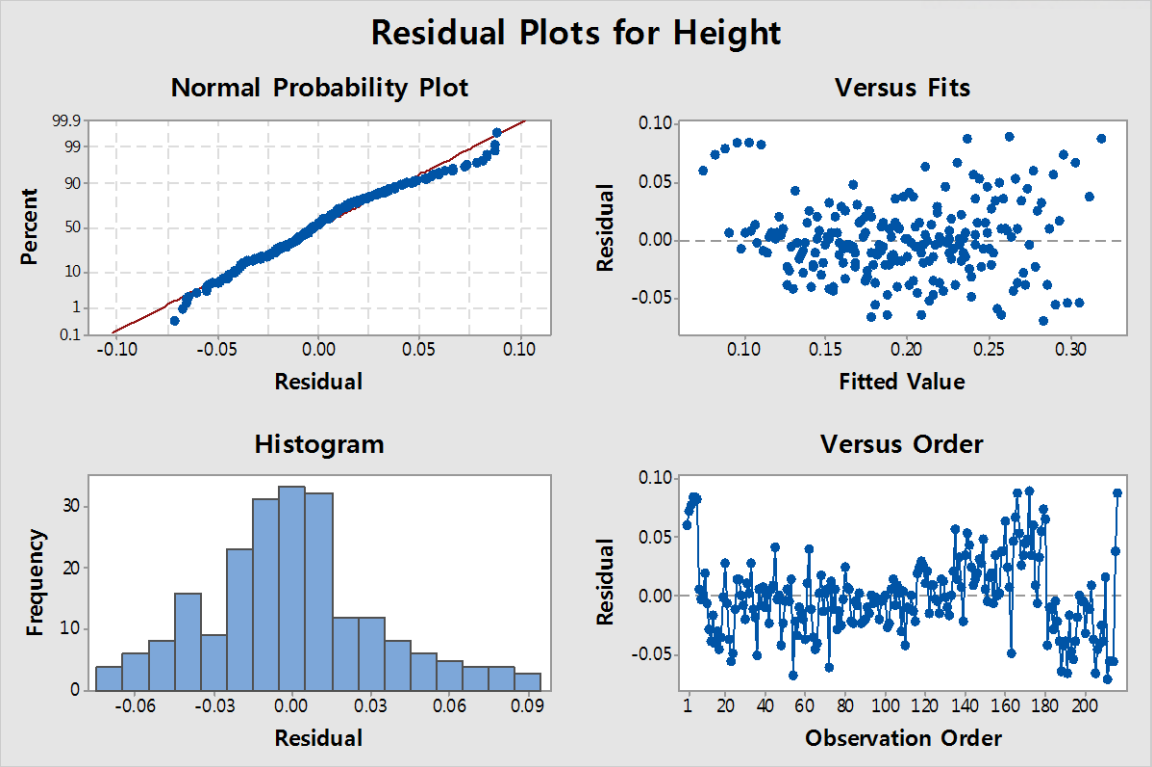

Figure 3.13 Residual plots for height

3.2.3 Optimization of process parameters

Target dimension

The target dimension value is 0.25 mm thick on one layer or 0.25 mm high on the multi-track. The width of the single track is between 0.8 mm and 1.0 mm, since the diameter of the laser beam is 0.8mm.

Single track

First, only 350W of laser power was satisfied as shown in Figure 3.14. Then four parameters of PFR 4.5,5.5,6.5,7.5 g/min entered the range when looking at dispersion by powder feed rate to tracks printed at 350 W in Figure 3.15.

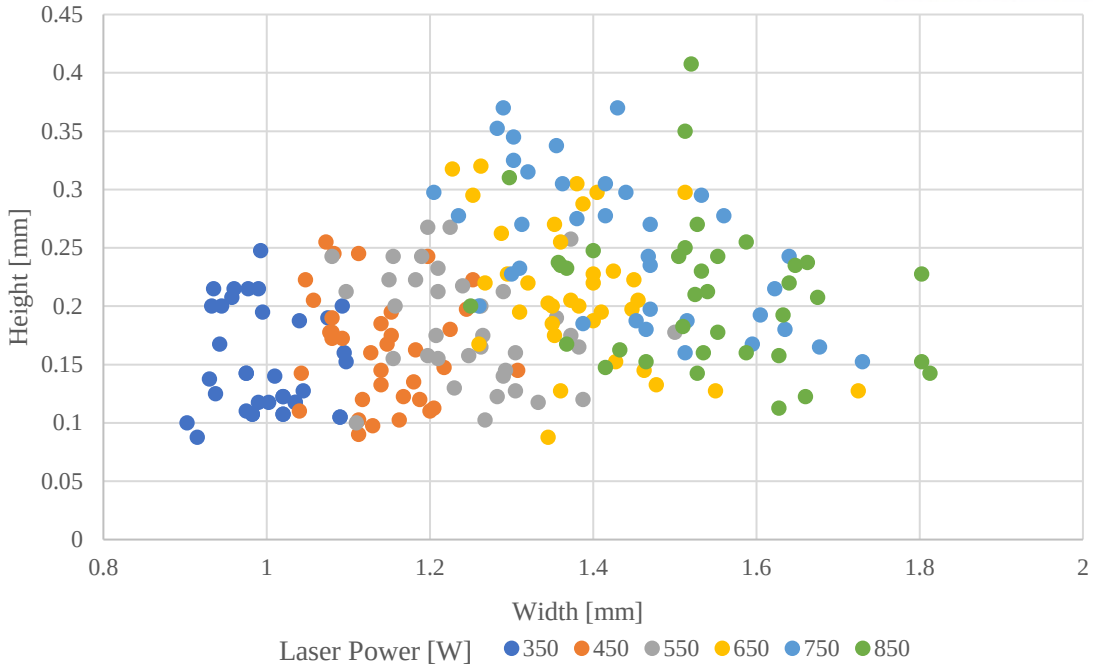

Figure 3.14 Width and height according to laser power

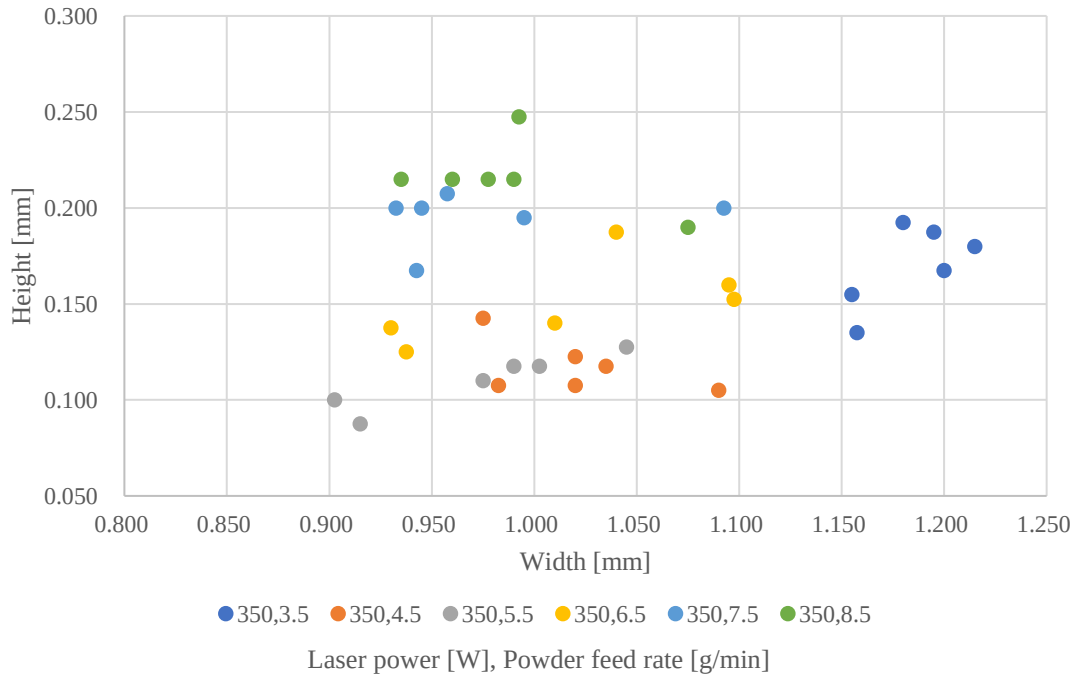

Figure 3.15 Width and height according to powder feed rate at laser power 350W

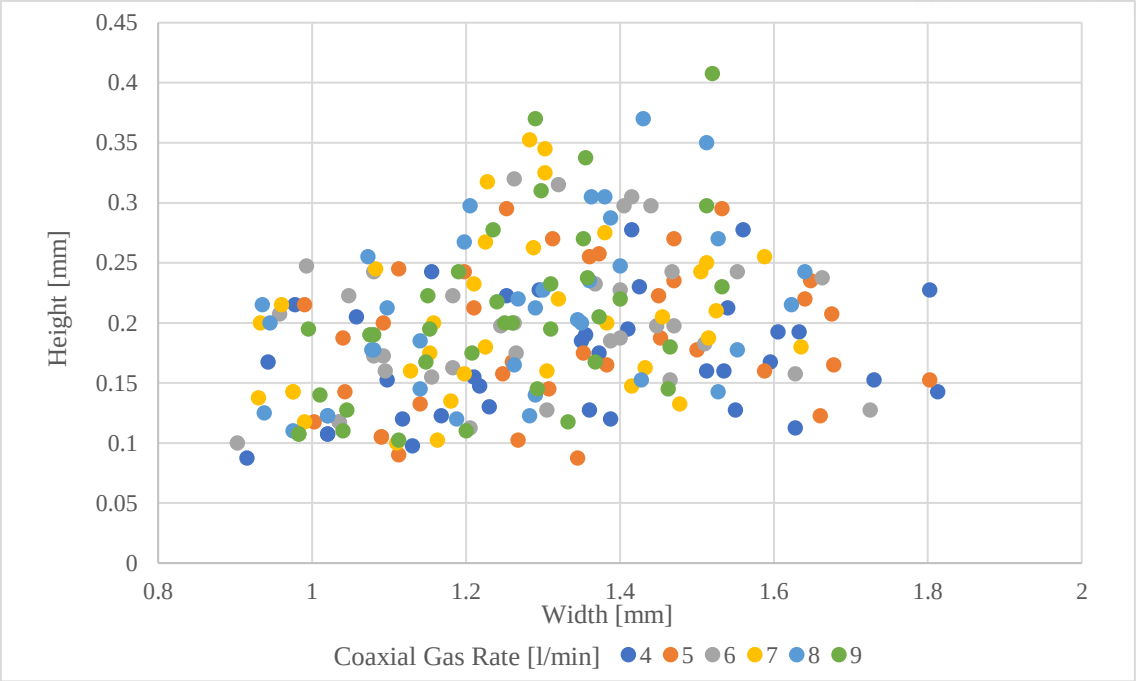

Figure 3.16 Width and height according to coaxial gas rate

Multi track

It was able to narrow the range of process parameters by PFR 4.5-7.5, CGR 7, and LP350 in single track. Then, as shown in Figure 3.14, for 4, 4.5, 5, 5.5, 6,6.5 7, 7.5g/min, 3mm additive test to reduce time and material. Exceeded height criteria during multi-layer stacking for 4, 6, 6.5, 7, 7.5 g/min. Resetting parameters in detail (0.1 units) only to meet the target conditions of a single-track result. Multi-track is printed with PFR 4.5-5.5g/min, CGR 7l/min, LP 350W as shown in Figure 3.15. The printed sample was cut in half and observed after micron polishing as shown in Figure 3.16. At the Powder feed rate 4.5, 4.8 g/min, as shown in Table 3.8, the height of the multi-track was measured closest to the target of more than 0.25 mm.

Figure 3.17 3mm additive test

Figure 3.18 Actual deposited geometry of multi-track

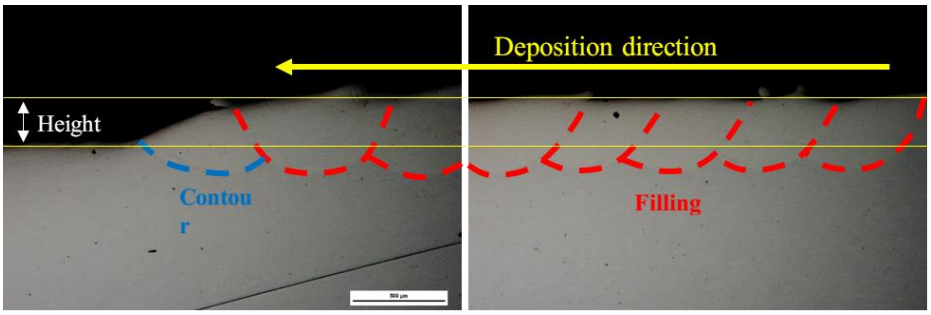

Figure 3.19 Multi track cross section

Table 3.8 Height of multi-track

PFR[g/min]	Height[mm]
4.5	**0.252**
4.6	0.212
4.7	0.246
4.8	**0.256**
4.9	0.268
5.0	0.199
5.1	0.376
5.2	0.335
5.3	0.293
5.4	0.279
5.5	0.326

Multi layer

It reduced process parameters to PFR 4.5g/min and 4.8g/min, CGR 7l/min, LP 350W on multi-track. For comparison, a total of four 20×20×20mm multilayer specimens were stacked up to PFR 4.2g/min and 5.1g/min. The relative density of XY, YZ Plane measured after micro polishing. PFR 5.1g/min did not meet the 20 mm height. For relative density, it showed the highest performance at PFR 4.8g/min out of the remaining three parameters. Therefore, the optimal process parameter was chosen as PFR 4.8g/min, CGR 7l/min, LP 350W.

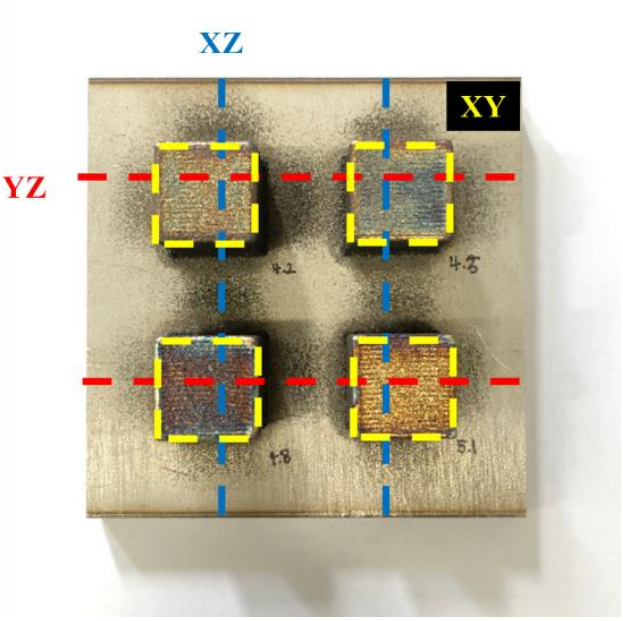

Figure 3.20 Actual deposited geometry of multi-layer

Table 3.9 Dimension of multi-layer

PFR[g/min]	X length [mm]	Y length [mm]	Z Height [mm]
4.2	21.06	21.11	20.18
4.5	21.13	21.13	20.04
4.8	21.16	21.23	20.17
5.1	21.25	21.29	19.95

Table 3.10 Relative density in multi-layer

PFR [g/min]	Relative density [%]			
	XY plane		YZ plane	
4.2	99.9554	Max. 99.978 Min. 99.937	99.974	Max. 99.979 Min. 99.959
4.5	99.9296	Max. 99.962 Min. 99.902	99.9704	Max. 99.985 Min. 99.954
4.8	99.9862	Max. 99.994 Min. 99.981	99.9872	Max. 99.995 Min. 99.981
5.1	99.9902	Max. 99.997 Min. 99.983	99.977	Max. 99.985 Min. 99.959

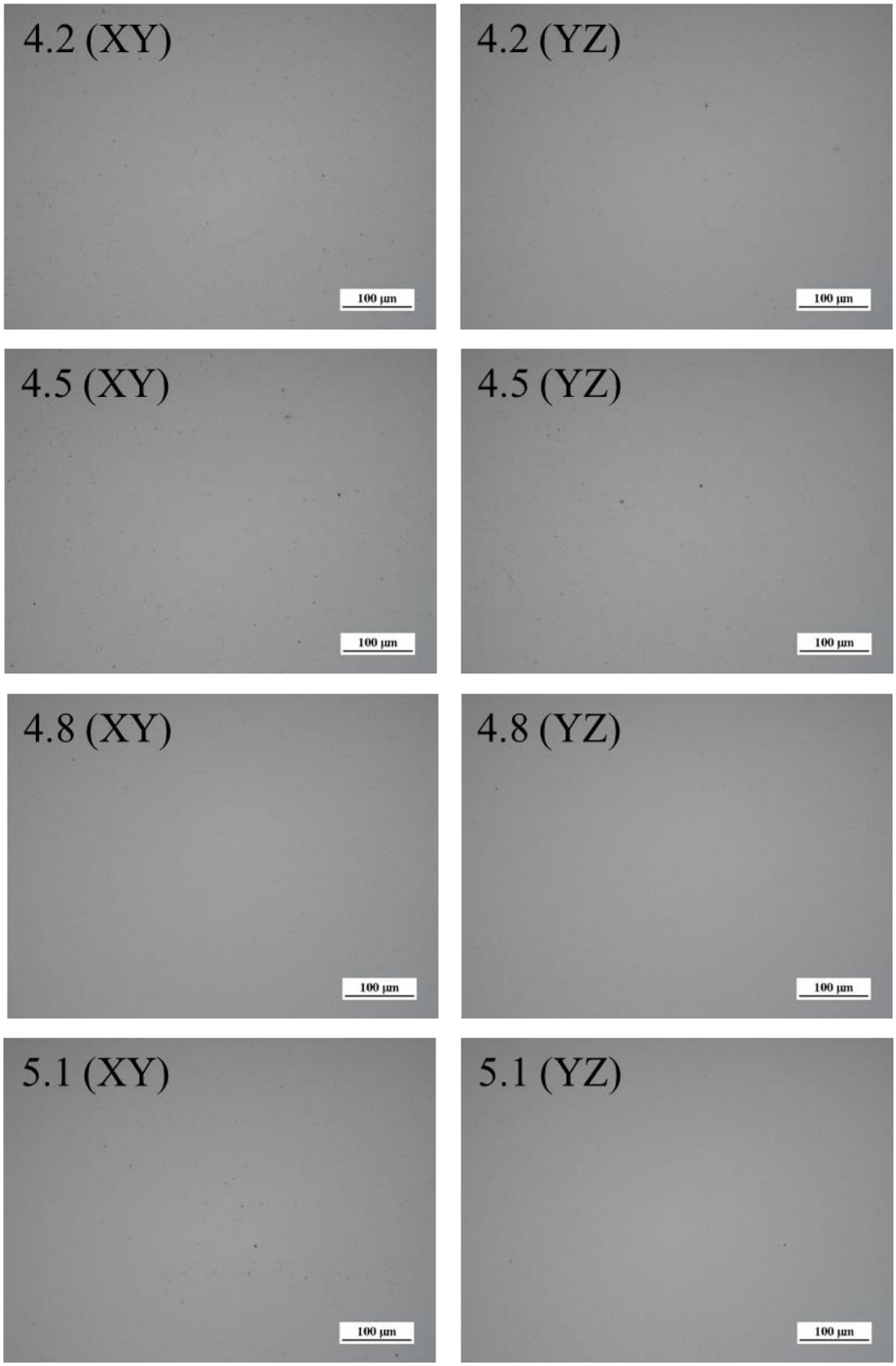

Figure 3.21 cross section of multi-layer

3.2.4 Mechanical properties of optimal process parameters

Using PFR 4.8g/min, CGR 7l/min, LP 350W, three specimens were produced for tensile and impact testing, and the specimens were manufactured on the condition of PFR 4.5g/min for comparison as shown in Figure 3.19. As shown in Table 3.11 and 3.12, DED Specimens yield strength is about twice as high as casting. It is estimated that the reason for the relatively low elongation rate of the DED specimen is due to its yield strength. Impact test results show better results than casting products under both conditions. Comparing the reproducibility (standard deviation) of the material properties with the mean value, it is judged that the powder feed rate of 4.8 g/min is more stable and better material properties than 4.5g/min can be reproduced.

The height and width of the single-track output with this process parameter was 0.94 mm high and 0.168mm wide, and the height and width of the munt track was 0.256mm and 11.168mm. In addition, the best results were obtained in the multi-layer, with a height of 20.17mm and a relative density of 99.9872%.

Figure 3.22 Tensile and impact test specimens

Table 3.11 Results of tensile test

Condition	UTS [MPa]	YS [MPa]	Elongation [%]
4.5g/min	540.67(±21.08)	379(±3)	37.6(±2.12)
4.8g/min	577.04(±1.57)	413.54(±0.99)	50.31(±2.79)
Casting	515	205	60

Table 3.12 Results of impact test

Condition	Absorption energy [J]
4.5g/min	145.4(±1.04)
4.8g/min	140.37(±0.93)
Casting	515

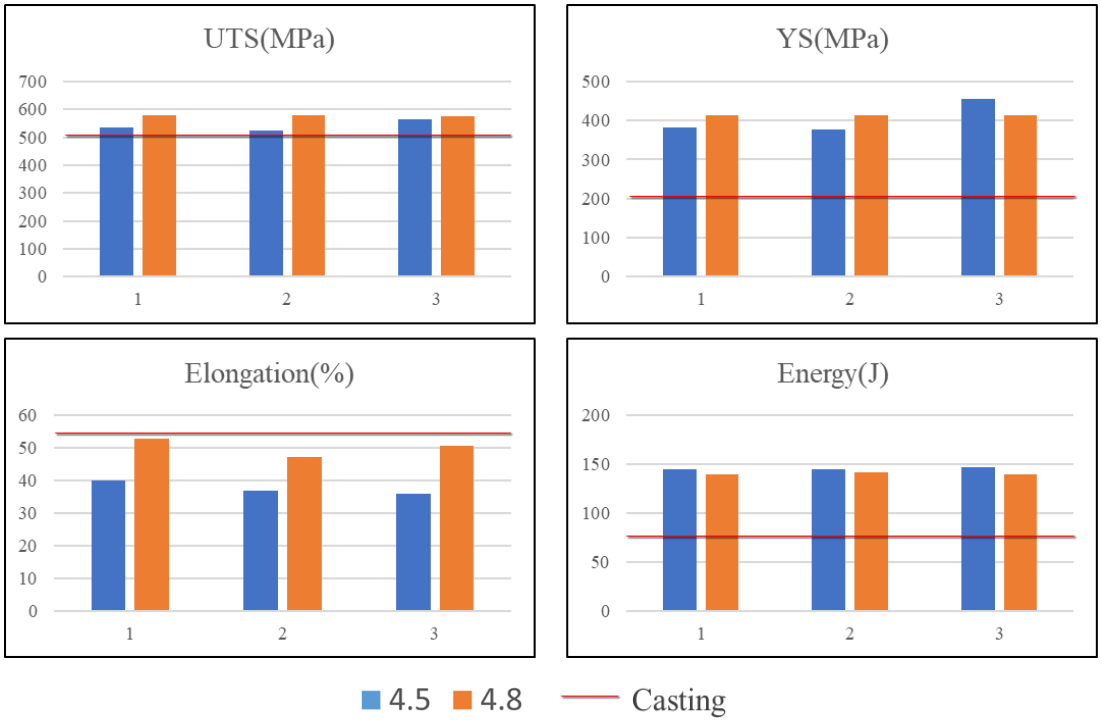

Figure 3.23 Plot of tensile and impact test results

Using PFR 4.8g/min, CGR 7l/min, LP 350W, ten specimens were produced and tested for fatigue testing as shown in Figure 3.24. The fatigue test was conducted at the stress ratio of -1, and frequency of 20 Hz after polishing. Using the MTS 810 machine, fatigue test was carried out up to 10^6 cycle by decreasing the stress by 25MPa from 400MPa. As a result, life cycle was identified more than 10^6 cycle at 300MPa as shown in Figure 3.25.

Figure 3.24 Specimens for fatigue test

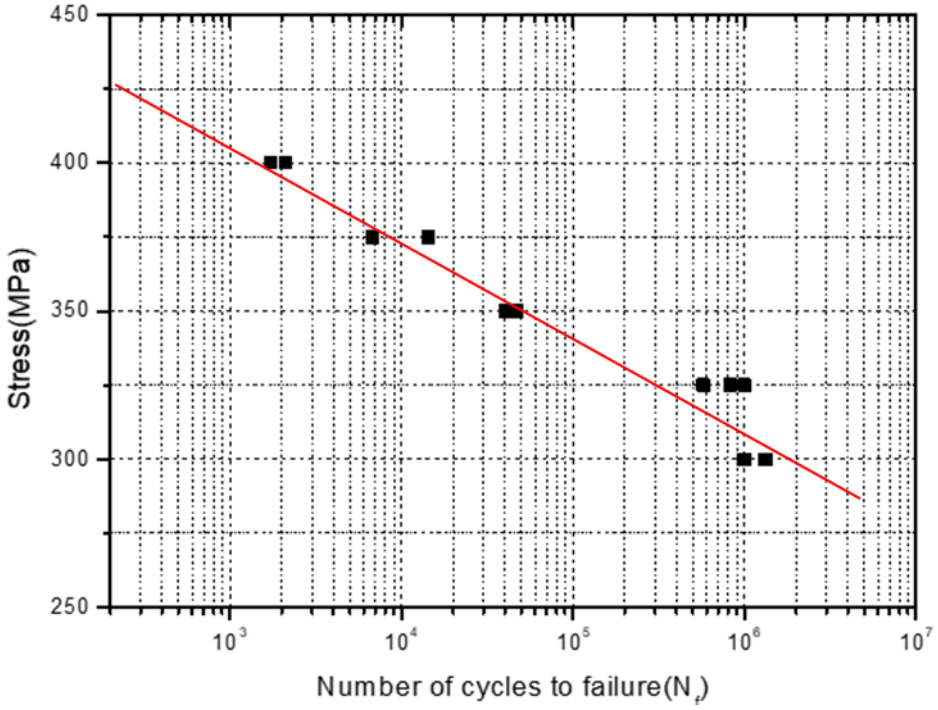

Figure 3.25 Result of fatigue test

3.3 Results and discussion

Physically the output from the DED process is an accumulation of single tracks Single track overlaps, creating a layer with multi-track, and then superimposed layers to complete with multi-layer output. As discussed in Chapter 2, the way the DED process outputs overlaps single and multi-track depending on the hatching space and layer thickness entered. The overlap ratio and the dilution depth produced will have a comprehensive effect on the dimensions and density of the final output. Thus, the analysis of the process parameters in the bulk model was combined with too many parameters and, when the analysis was conducted in the same way as Section 3.1, it was found that it was difficult to analyze the effects of each parameter, as was the result that the height was significant for all parameters. In the case of the relative density, its significance is proved not to be enough for all parameters while the relative density is greater than 99.95% for all treatment in the experiment space. Thus, it is acceptable when the product is manufactured using typical metal manufacturing process.

In contrast, the process in section 3.2 confirmed how single tracks accumulate in multi-track, multi-layer and affect the output. It was found through multi-scale analysis that the effects of existing input parameters on single track, multi-track, and multilayer did not simply increase or decrease on multi-scale, but produced an integrated result, and that overlap ratio, which was not known in bulk models, affected dimensions by the accumulation of tracks. As expected, the overlap of the single track confirms that the height of the multi-track is higher than the height of the single track single and the width between peaks has not changed.

Comparing the optimal process parameters obtained in section 3.1 and 3.2, is show in Table 3.13.

Table 3.13 optimal process parameters derived by different samples

	Bulk samples	Multi-scale samples
PFR [g/min]	4.8566	4.8000
LP [W]	400	350
CGR [l/min]	6.5	7

PFR is much more significant than LP and CGR, as shown in Figure 3.5 of Section 3.1. Considering this point, the optimal process parameter values using multi-scale samples were found to be valid because the values of the optimized process parameters using bulk samples and the

values of the optimized process parameters using multi-scale samples were almost identical. In addition, multi - scale samples using materials and time by 83 % used in the optimization way. Based on the sample output, the Bulk Samples method took 27 hours, and the multi-scale samples took about 4 hours and 30 minutes. The output based on the 20×20×20mm cube sample took one hour, and the three-level designs were made for the three parameters, resulting in a total of 27 specimens being produced, which took 27 hours. A six-level design of three parameters on one side produced 216 single track and 11 multi-track four multi-layer specimens, which took 4 hours and 30 minutes based on pure power time. Moreover, it can be said that the material cost was reduced by 83% due to the proportional consumption of materials in time due to the nature of the DED process.

The optimal process parameters are verified for mechanical properties through tensile and impact tests. Specimens yield strength is about twice as high as casting. It is estimated that the reason for the relatively low elongation rate of the DED specimen is due to its yield strength. Impact test results show better results than casting products under both conditions. Additionally, the fatigue limit is about 35% of the tensile strength at 10^7 cycle for ASTM A276. As shown in S-N curve of Figure 3.2, it can be inferred that the fatigue limit is higher than 250MPa at 10^7 cycle. These show that the optimal process parameters found by the methods presented can be applications as target products.

4. Conclusion

This study aims to analyze fundamental parameters of the DED process on mechanical properties of printed parts, whereas previous studies typically used bulk models to directly investigate the effects of process parameters on final products. Grounded on the fact that a printed product is the aggregated single tracks, the effect of input process parameters (laser power, powder feed rate and coaxial gas rate) was analyzed on width, height and relative density using the scale divided across single track, multi-track and multi-layer. All specimens are printed on the fixed experimental setting of the DED machine (i.e., MX-600) of which powder and substrate are SUS316L.

Despite the need for further analysis, multi-scale analysis has shown the possibility of predicting the quality of the final product. The sequential analysis of single track, multi-track and multi-layer resulted in the almost same result as the bulk samples analysis by viewing the process of single-track aggregation being changed into multi-layer. The optimal process parameter was derived by bulk samples (powder feed rate 4.8566g/min, laser power 300W, coaxial gas rate 6.5l/min) and multi-scale samples (powder feed rate 4.8g/min, laser power 350W, coaxial gas rate 7.0l/min). The two values are similar, especially the powder feed rate, which has the most significant effect on dimensional accuracy. This obtained process parameters also showed excellent performance in mechanical properties.

DED has recently emerged as a key tool in product manufacturing beyond mold repair in the metal 3D printing sector. However, due to the nature of the DED process, it is difficult to apply it as an industry in a cost-effective way by using high-volume metal powder and high-power laser source Although a limited result, this study suggests an optimization method that reduces material and time costs of optimization by 83%. This can be seen as a steppingstone to optimize the quality of the final product with a single track alone. For this, further analysis is required of how the relationship between single track, multi-track and multi-layer, overlap ratio, and dilution change with process pars. In addition, depending on the application area, optimization of various properties, such as tensile strength and fatigue life, will be required, which can be improved through multi-objective optimization techniques such as Pareto Optimal.

Reference

[1] Wohlers, T., et al., *Wohlers Report 2018*. 2018, Wohlers Associates.

[2] Shamsaei, N., Yadollahi, A., Bian, L., & Thompson, S. M. (2015). An overview of Direct Laser Deposition for additive manufacturing; Part II: Mechanical behavior, process parameter optimization and control. *Additive Manufacturing, 8, 12-35. doi:10.1016/j.addma.2015.07.002*

[3] Yang, H., Kong, Z., & Sarder, M. D. (2016). Additive Manufacturing: A New Paradigm For Manufacturing. In Proceedings of the 2016 Industrial and Systems Engineering Research Conference, Availability, Development (Vol. 14, p. 102).

[4] Moodleah, S., Bohez, E. J., & Makhanov, S. S. (2016). Five-axis machining of STL surfaces by adaptive curvilinear toolpaths. International Journal of Production Research, 54(24), 7296-7329.

[5] Gou, G., Zhang, M., Chen, H., Chen, J., Li, P., & Yang, Y. P. (2015). Effect of humidity on porosity, microstructure, and fatigue strength of A7N01S-T5 aluminum alloy welded joints in high-speed trains. Materials & Design, 85, 309-317.

[6] ASTM (2012). Addtive manufacturing – General principles – Terminology. In (Vol. ISO/ASTM 52900:2015)

[7] Sidambe, A. (2014). Biocompatibility of Advanced Manufactured Titanium Implants – A Review. *Materials*, 7(12), 8168-8188. Doi:10.3390/ma7128168

[8] Gardan, J. (2015). Additive mnaufacturing technologies: statae of the art and trends. International Journal of Production Research, 54(10), 1-15. Doi:10.1080/00207543.2015.1115909

[9] Shamsaei, N., Yadollahi, A., Bian, L., & Thompson, S. M. (2015). An overview of Direct Laser Deposition for additive manufacturing; Part I: Transport phenomena, modeling and diagnostics. *Additive Manufacturing, 8, 12-35. doi:10.1016/j.addma.2015.07.002*

[10] Milewski, J. O. (2017). Additive manufacturing of metals: from fundamental technology to rocket nozzles, medical implants, and custom jewelry (Vol. 258). Springer.

[11] Gibson, I. (2010) *Additive manufacturing Technologies Rapid prototyping to Direct Digital Manufacturing*: Boston, MA: Springer US: Imprint: Springer

[12] Ya, W. (2015). Laser materials interactions during cladding: analyses on clad formation, thermal cycles, residual stress and defects.

[13] Yao, Y., et al. (2018). Influence of processing parameters and heat treatment on the mechanical properties of 18Ni300 manufactured by laser based directed energy deposition. Optics & Laser Technology 105: 171-179.

[14] El Cheikh, H., Courant, B., Branchu, S., Hascoët, J. Y., & Guillén, R. (2012). Analysis and

prediction of single laser tracks geometrical characteristics in coaxial laser cladding process. *Optics and Lasers in Engineering, 50(3), 413-422. doi:10.1016/j.optlaseng.2011.10.014*

[15] El Cheikh, H., Courant, B., Branchu, S., Huang, X., Hascoët, J.-Y., & Guillén, R. (2012). Prediction and analytical description of the single laser track geometry in direct laser fabrication from process parameters and energy balance reasoning. *Journal of Materials Processing Technology, 212(9), 1832-1839. doi:10.1016/j.jmatprotec.2012.03.016*

[16] El Cheikh, H., Courant, B., Branchu, S., Huang, X., Hascoët, J.-Y., & Guillén, R. (2012). Direct Laser Fabrication process with coaxial powder projection of 316L steel. Geometrical characteristics and microstructure characterization of wall structures. *Optics and Lasers in Engineering, 50(12), 1779-1784. doi:10.1016/j.optlaseng.2012.07.002*

[17] Hwang, J.-H., Shin, S.-S., Jung, G.-I., Kim, S.-W., & Kim, H.-D. (2016). A Study on the Characteristics of Laser Deposition Surface and Cross-section for Metal Powder. *Journal of Welding and Joining, 34(4), 17-22. doi:10.5781/jwj.2016.34.4.17*

[18] Hwang, J., Shin, S., Lee, J., Kim, S., & Kim, H. (2017). A Study on Surface and Cross-section Properties Depending on the Process Parameters of Laser Depositions with Metal Powders (SUS316L and IN718). *Journal of Welding and Joining, 35(3), 28-34. doi:10.5781/jwj.2017.35.3.5*

[19] Bax, B., Rajput, R., Kellet, R., & Reisacher, M. (2018). Systematic evaluation of process parameter maps for laser cladding and directed energy deposition. *Additive Manufacturing, 21, 487-494. doi:10.1016/j.addma.2018.04.002*

[20] Yu, J., Lin, X., Ma, L., Wang, J., Fu, X., Chen, J., & Huang, W. (2011). Influence of laser deposition patterns on part distortion, interior quality and mechanical properties by laser solid forming (LSF). *Materials Science and Engineering: A, 528(3), 1094-1104. doi:10.1016/j.msea.2010.09.078*

[21] Shim, D.-S., Baek, G.-Y., Seo, J.-S., Shin, G.-Y., Kim, K.-P., & Lee, K.-Y. (2016). Effect of layer thickness setting on deposition characteristics in direct energy deposition (DED) process. *Optics & Laser Technology, 86, 69-78. doi:10.1016/j.optlastec.2016.07.001*

[22] Izadi, M., Farzaneh, A., Gibson, I., & Rolfe, B. (2018). The effect of process parameters and mechanical properties of direct energy deposition stainless steel.

[23] Jeon, T., Hwang, T., Yun, H., VanTyne, C., & Moon, Y. (2018). Control of Porosity in Parts Produced by a Direct Laser Melting Process. *Applied Sciences, 8(12). doi:10.3390/app8122573*

[24] Sciammarella, F., & Salehi Najafabadi, B. (2018). Processing Parameter DOE for 316L Using Directed Energy Deposition. *Journal of Manufacturing and Materials Processing, 2(3). doi:10.3390/jmmp2030061*

[25] Baek, G. Y., Shin, G. Y., Lee, K. Y., & Shim, D. S. (2019). Mechanical Properties of Tool

Steels with High Wear Resistance via Directed Energy Deposition. *Metals, 9(3). doi:10.3390/met9030282*

[26] Tan, Z. E. E., Pang, J. H. L., Kaminski, J., & Pepin, H. (2019). Characterisation of porosity, density, and microstructure of directed energy deposited stainless steel AISI 316L. *Additive Manufacturing, 25, 286-296. doi:10.1016/j.addma.2018.11.014*

[27] Weng, F., Gao, S., Jiang, J., Wang, J., & Guo, P. (2019). A novel strategy to fabricate thin 316L stainless steel rods by continuous directed energy deposition in Z direction. *Additive Manufacturing, 27, 474-481. doi:10.1016/j.addma.2019.03.024*

[28] Ren, K., Chew, Y., Zhang, Y. F., Bi, G. J., & Fuh, J. Y. H. (2019). Thermal analyses for optimal scanning pattern evaluation in laser aided additive manufacturing. Journal of Materials Processing Technology, 271, 178-188. doi:10.1016/j.jmatprotec.2019.03.029

[29] Ren, K., Chew, Y., Fuh, J. Y. H., Zhang, Y. F., & Bi, G. J. (2019). Thermo-mechanical analyses for optimized path planning in laser aided additive manufacturing processes. *Materials & Design, 162, 80-93. doi:10.1016/j.matdes.2018.11.014*

[30] Nickel, A. H., Barnett, D. M., & Prinz, F. B. (2001). Thermal stresses and deposition patterns in layered manufacturing.

[31] Dai, K., & Shaw, L. (2002). Distortion minimization of laser-processed components through control of laser scanning patterns. *Rapid Prototyping Journal, 8(5), 270-276. doi:10.1108/13552540210451732*

[32] Nam, S., Cho, H., Kim, C., & Kim, Y.-M. (2018). Effect of Process Parameters on Deposition Properties of Functionally Graded STS 316/Fe Manufactured by Laser Direct Metal Deposition. Metals, 8(8). doi:10.3390/met8080607

[33] Oh, W. J., Lee, W. J., Kim, M. S., Jeon, J. B., & Shim, D. S. (2019). Repairing additive-manufactured 316L stainless steel using direct energy deposition. Optics & Laser Technology, 117, 6-17. doi:10.1016/j.optlastec.2019.04.012

Appendix A: MX-600 specification

Table A.1 Technical data

Laser type Ytterbium Fiber laser	Max. 1,000 W
Machine size	2000(W)×2900(L) ×2550(H) mm
Machine weigh	6,500 kg
Gas	Argon (>99.999%)

Table A.2 Axes main specification

X, Y, Z Linear Motion System			
Item	Axis	Unit	Specification
Stroke	X	mm	450
	Y	mm	600
	Z	mm	380
Rapid traverse	X	mm/s	200
	Y	mm/s	200
	Z	mm/s	150

A & C (Tilt & Rotating table System)			
Item	Unit	Specification	
		A- aixs (Tilt-axis)	C- aixs (Rotary-axis)
Axis travel	Deg. (°)	-100 ~ +5	360
Rapid speed	RPM	30	60
Table size	mm	Ø 350 / 600x500	
Permission mass of work piece	Kg	Horizontal	Vertical
		300	150

Appendix B: Width, height and relative density of cubes

PFR [g/min]	LP [W]	CGR [l/min]	X [mm]	Y [mm]	Z [mm]	RD [%]
4.5	300	6.5	16.37	16.33	14.79	99.9516
4.5	300	7	16.34	16.31	14.82	99.9604
4.5	300	7.5	16.42	16.33	15.06	99.9886
4.5	350	6.5	16.4	16.37	14.71	99.9524
4.5	350	7	16.39	16.29	14.82	99.9668
4.5	350	7.5	16.36	16.31	14.83	99.9672
4.5	400	6.5	16.45	16.35	14.85	99.9492
4.5	400	7	16.42	16.32	14.99	99.98
4.5	400	7.5	16.41	16.31	14.83	99.9844
5	300	6.5	16.29	16.34	15.11	99.9792
5	300	7	16.37	16.35	15.13	99.9282
5	300	7.5	16.49	16.36	15.18	99.9316
5	350	6.5	16.53	16.34	15.04	99.9124
5	350	7	16.46	16.3	15.07	99.9708
5	350	7.5	16.42	16.37	14.86	99.9862
5	400	6.5	16.52	16.33	15.18	99.9702
5	400	7	16.34	16.34	15.17	99.978
5	400	7.5	16.45	16.31	14.82	99.9576
5.5	300	6.5	16.35	16.29	15.54	99.9084
5.5	300	7	16.25	16.2	15.39	99.9834
5.5	300	7.5	16.26	16.27	15.33	99.9848
5.5	350	6.5	16.26	16.24	15.23	99.9852
5.5	350	7	16.27	16.32	15.3	99.971
5.5	350	7.5	16.29	16.29	15.4	99.987
5.5	400	6.5	16.23	16.22	15.31	99.9664
5.5	400	7	16.39	16.2	15.34	99.9764
5.5	400	7.5	16.38	16.22	15.52	99.9804

Appendix C: Width and height of single tracks

LP [W]	PFR [g/min]	CGR [l/min]	Width [mm]	Height [mm]
350	3.5	4.0	0.9475	0.0750
350	3.5	5.0	0.9650	0.1000
350	3.5	6.0	0.9800	0.0800
350	3.5	7.0	1.1200	0.1025
350	3.5	8.0	0.9050	0.0900
350	3.5	9.0	0.9000	0.0750
350	4.5	4.0	1.0200	0.1075
350	4.5	5.0	1.0900	0.1050
350	4.5	6.0	1.0350	0.1175
350	4.5	7.0	0.9750	0.1425
350	4.5	8.0	1.0200	0.1225
350	4.5	9.0	0.9825	0.1075
350	5.5	4.0	0.9150	0.0875
350	5.5	5.0	1.0025	0.1175
350	5.5	6.0	0.9025	0.1000
350	5.5	7.0	0.9900	0.1175
350	5.5	8.0	0.9750	0.1100
350	5.5	9.0	1.0450	0.1275
350	6.5	4.0	1.0975	0.1525
350	6.5	5.0	1.0400	0.1875
350	6.5	6.0	1.0950	0.1600
350	6.5	7.0	0.9300	0.1375
350	6.5	8.0	0.9375	0.1250
350	6.5	9.0	1.0100	0.1400
350	7.5	4.0	0.9425	0.1675
350	7.5	5.0	1.0925	0.2000
350	7.5	6.0	0.9575	0.2075
350	7.5	7.0	0.9325	0.2000
350	7.5	8.0	0.9450	0.2000
350	7.5	9.0	0.9950	0.1950
350	8.5	4.0	0.9775	0.2150
350	8.5	5.0	0.9900	0.2150
350	8.5	6.0	0.9925	0.2475
350	8.5	7.0	0.9600	0.2150
350	8.5	8.0	0.9350	0.2150

350	8.5	9.0	1.0750	0.1900
450	3.5	4.0	1.1300	0.0975
450	3.5	5.0	1.1125	0.0900
450	3.5	6.0	1.2050	0.1125
450	3.5	7.0	1.1625	0.1025
450	3.5	8.0	1.1875	0.1200
450	3.5	9.0	1.1125	0.1025
450	4.5	4.0	1.1675	0.1225
450	4.5	5.0	1.1400	0.1325
450	4.5	6.0	1.0925	0.1725
450	4.5	7.0	1.1800	0.1350
450	4.5	8.0	1.1400	0.1450
450	4.5	9.0	1.0400	0.1100
450	5.5	4.0	1.1175	0.1200
450	5.5	5.0	1.3075	0.1450
450	5.5	6.0	1.1825	0.1625
450	5.5	7.0	1.1275	0.1600
450	5.5	8.0	1.1400	0.1850
450	5.5	9.0	1.2000	0.1100
450	6.5	4.0	1.2175	0.1475
450	6.5	5.0	1.0425	0.1425
450	6.5	6.0	1.0800	0.1725
450	6.5	7.0	1.1525	0.1750
450	6.5	8.0	1.0775	0.1775
450	6.5	9.0	1.1475	0.1675
450	7.5	4.0	1.0575	0.2050
450	7.5	5.0	1.1975	0.2425
450	7.5	6.0	1.2450	0.1975
450	7.5	7.0	1.2250	0.1800
450	7.5	8.0	1.0800	0.1775
450	7.5	9.0	1.0800	0.1900
450	8.5	4.0	1.2525	0.2225
450	8.5	5.0	1.1125	0.2450
450	8.5	6.0	1.0475	0.2225
450	8.5	7.0	1.0825	0.2450
450	8.5	8.0	1.0725	0.2550
450	8.5	9.0	1.1525	0.1950
550	3.5	4.0	1.3875	0.1200
550	3.5	5.0	1.2675	0.1025

550	3.5	6.0	1.3050	0.1275
550	3.5	7.0	1.1100	0.1000
550	3.5	8.0	1.2825	0.1225
550	3.5	9.0	1.3325	0.1175
550	4.5	4.0	1.2300	0.1300
550	4.5	5.0	1.3825	0.1650
550	4.5	6.0	1.1550	0.1550
550	4.5	7.0	1.3050	0.1600
550	4.5	8.0	1.2900	0.1400
550	4.5	9.0	1.2925	0.1450
550	5.5	4.0	1.2100	0.1550
550	5.5	5.0	1.2475	0.1575
550	5.5	6.0	1.2650	0.1750
550	5.5	7.0	1.1975	0.1575
550	5.5	8.0	1.2625	0.1650
550	5.5	9.0	1.2075	0.1750
550	6.5	4.0	1.3725	0.1750
550	6.5	5.0	1.5000	0.1775
550	6.5	6.0	1.2625	0.2000
550	6.5	7.0	1.1575	0.2000
550	6.5	8.0	1.2900	0.2125
550	6.5	9.0	1.2400	0.2175
550	7.5	4.0	1.3550	0.1900
550	7.5	5.0	1.2100	0.2125
550	7.5	6.0	1.1825	0.2225
550	7.5	7.0	1.2100	0.2325
550	7.5	8.0	1.0975	0.2125
550	7.5	9.0	1.1500	0.2225
550	8.5	4.0	1.1550	0.2425
550	8.5	5.0	1.3725	0.2575
550	8.5	6.0	1.0800	0.2425
550	8.5	7.0	1.2250	0.2675
550	8.5	8.0	1.1975	0.2675
550	8.5	9.0	1.1900	0.2425
650	3.5	4.0	1.5500	0.1275
650	3.5	5.0	1.3450	0.0875
650	3.5	6.0	1.7250	0.1275
650	3.5	7.0	1.4775	0.1325
650	3.5	8.0	1.4275	0.1525

650	3.5	9.0	1.4625	0.1450
650	4.5	4.0	1.3600	0.1275
650	4.5	5.0	1.3525	0.1750
650	4.5	6.0	1.4000	0.1875
650	4.5	7.0	1.3825	0.2000
650	4.5	8.0	1.3450	0.2025
650	4.5	9.0	1.3100	0.1950
650	5.5	4.0	1.4100	0.1950
650	5.5	5.0	1.2600	0.1675
650	5.5	6.0	1.4475	0.1975
650	5.5	7.0	1.4550	0.2050
650	5.5	8.0	1.3500	0.2000
650	5.5	9.0	1.3725	0.2050
650	6.5	4.0	1.3500	0.1850
650	6.5	5.0	1.4500	0.2225
650	6.5	6.0	1.4000	0.2275
650	6.5	7.0	1.3200	0.2200
650	6.5	8.0	1.2675	0.2200
650	6.5	9.0	1.4000	0.2200
650	7.5	4.0	1.2950	0.2275
650	7.5	5.0	1.3600	0.2550
650	7.5	6.0	1.4050	0.2975
650	7.5	7.0	1.2875	0.2625
650	7.5	8.0	1.3875	0.2875
650	7.5	9.0	1.3525	0.2700
650	8.5	4.0	1.4250	0.2300
650	8.5	5.0	1.2525	0.2950
650	8.5	6.0	1.2625	0.3200
650	8.5	7.0	1.2275	0.3175
650	8.5	8.0	1.3800	0.3050
650	8.5	9.0	1.5125	0.2975
750	3.5	4.0	1.7300	0.1525
750	3.5	5.0	1.6775	0.1650
750	3.5	6.0	1.3875	0.1850
750	3.5	7.0	1.5150	0.1875
750	3.5	8.0	1.6225	0.2150
750	3.5	9.0	1.4650	0.1800
750	4.5	4.0	1.5125	0.1600
750	4.5	5.0	1.4525	0.1875

750	4.5	6.0	1.4700	0.1975
750	4.5	7.0	1.6350	0.1800
750	4.5	8.0	1.3000	0.2275
750	4.5	9.0	1.2600	0.2000
750	5.5	4.0	1.6050	0.1925
750	5.5	5.0	1.4700	0.2350
750	5.5	6.0	1.4675	0.2425
750	5.5	7.0	1.3800	0.2750
750	5.5	8.0	1.6400	0.2425
750	5.5	9.0	1.3100	0.2325
750	6.5	4.0	1.5950	0.1675
750	6.5	5.0	1.3125	0.2700
750	6.5	6.0	1.4400	0.2975
750	6.5	7.0	1.3025	0.3250
750	6.5	8.0	1.2050	0.2975
750	6.5	9.0	1.2350	0.2775
750	7.5	4.0	1.4150	0.2775
750	7.5	5.0	1.5325	0.2950
750	7.5	6.0	1.4150	0.3050
750	7.5	7.0	1.2825	0.3525
750	7.5	8.0	1.3625	0.3050
750	7.5	9.0	1.3550	0.3375
750	8.5	4.0	1.5600	0.2775
750	8.5	5.0	1.4700	0.2700
750	8.5	6.0	1.3200	0.3150
750	8.5	7.0	1.3025	0.3450
750	8.5	8.0	1.4300	0.3700
750	8.5	9.0	1.2900	0.3700
850	3.5	4.0	1.6275	0.1125
850	3.5	5.0	1.8025	0.1525
850	3.5	6.0	1.6275	0.1575
850	3.5	7.0	1.4150	0.1475
850	3.5	8.0	1.5525	0.1775
850	3.5	9.0	1.3675	0.1675
850	4.5	4.0	1.8125	0.1425
850	4.5	5.0	1.6600	0.1225
850	4.5	6.0	1.4650	0.1525
850	4.5	7.0	1.4325	0.1625
850	4.5	8.0	1.5275	0.1425

850	4.5	9.0	1.2500	0.2000
850	5.5	4.0	1.5350	0.1600
850	5.5	5.0	1.5875	0.1600
850	5.5	6.0	1.5100	0.1825
850	5.5	7.0	1.5250	0.2100
850	5.5	8.0	1.3600	0.2350
850	5.5	9.0	1.3575	0.2375
850	6.5	4.0	1.8025	0.2275
850	6.5	5.0	1.6750	0.2075
850	6.5	6.0	1.6625	0.2375
850	6.5	7.0	1.5050	0.2425
850	6.5	8.0	1.5275	0.2700
850	6.5	9.0	1.5325	0.2300
850	7.5	4.0	1.6325	0.1925
850	7.5	5.0	1.6400	0.2200
850	7.5	6.0	1.3675	0.2325
850	7.5	7.0	1.5875	0.2550
850	7.5	8.0	1.4000	0.2475
850	7.5	9.0	1.2975	0.3100
850	8.5	4.0	1.5400	0.2125
850	8.5	5.0	1.6475	0.2350
850	8.5	6.0	1.5525	0.2425
850	8.5	7.0	1.5125	0.2500
850	8.5	8.0	1.5125	0.3500
850	8.5	9.0	1.5200	0.4075

Appendix D: Width and height of multi tracks

	PFR [g/min]	Single track		Multi track	
		Width [mm]	Height [mm]	Width [mm]	Height [mm]
LP: 350W CGR: 7l/min	4.5	0.9775	0.1325	11.327	0.252
	4.6	0.9500	0.1475	10.916	0.212
	4.7	1.1250	0.1225	11.150	0.246
	4.8	0.9400	0.1675	11.168	0.256
	4.9	0.9725	0.1500	11.159	0.268
	5.0	1.0050	0.1375	11.093	0.199
	5.1	1.0350	0.1725	11.110	0.376
	5.2	0.9950	0.1400	10.888	0.335
	5.3	0.9675	0.1250	11.056	0.293
	5.4	1.0725	0.1850	11.056	0.279
	5.5	0.9475	0.1600	11.047	0.326

Acknowledgement

First, I appreciate advice and encouragement of my advisor, Prof. Namhun Kim, who has professional on additive manufacturing based on industrial engineering and mechanical engineering. Also, his trust and warmth helped me through my graduate course. And thank you to Prof. Duckyoung Kim and Prof. Youngbin Park, who are members of the thesis committee. I respect you all the time.

First, I sincerely appreciate my advisor, Prof. Namhun Kim for his guidance and encouragement. Also, his trust and warmth helped me through my undergraduate course and the master course. It was an honor to learn about additive manufacturing under the prof. Namjun Kim. And I appreciate committee members, Prof. Duckyoung Kim and Prof. Youngbin Park, who provide advice and support based on industrial engineering and mechanical engineering.

And I thank UCIM members. Dr. Eunjoo Park, Dr. Jooyeon Kwon, helped me grow as a researcher. Especially, Dr. Eunjoo Park filled my master's degree with generous encouragement and advice, thank you. Also, Moise, Young-gwang, Ikchan, Hweeyoung, Sangho, Jeongsik, Donghwan, Haejoon, Moon-yeong and Eunseo helped me adapt to my graduate school life. And Taeyang, Haekwon, Minsoo, and Jageon worked and studied with me day and night. Also, thank 3DAM center members.

Lastly, thank you to Ye-ji, Jeong-soon, Ji-yeon, Na-rae, Jun-hyuk, Hye-yeon, and Yoon-ho for many memories after entering UNIST. You are my youth, and I could graduate because of you And I thank my family for always supporting me.